

台灣顯微鏡學會

108年度會議暨第39屆學術研討會



日本電子株式会社
捷東股份有限公司

Solutions for Innovation

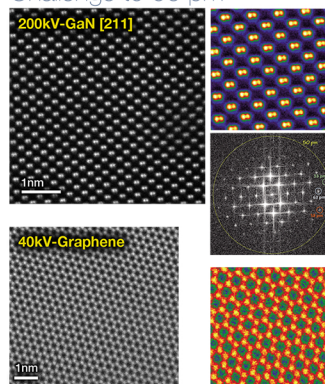
"NEOARM"

New Atomic Resolution Analytical Electron Microscope

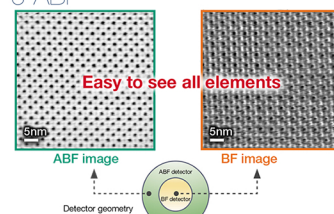
Ultimate Resolution powered by "Neo Engine" -

Cold FEG with NEO ASCOR(Advanced STEM Cs corrector)

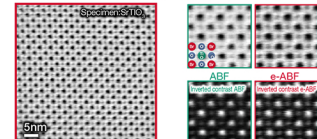
Ultimate Resolution
Challenge to 60 pm



Enhanced light atom contrast
e-ABF



"Real-time signal processing": $ABF - BF = e-ABF$



Easy to Tune Cs
JEOL COSMO™ Tune



Automated Aberration tuning including Higher order (up to 4th order)



Fast and accurate tuning
with no standard sample

Operate microscope in a bright room
Desktop EM



Camera for the viewing chamber is equipped as standard. Sample search, microscope alignment... all is doable just by looking at a PC monitor.

Resolution	STEM HAADF image	70 pm (200 kV), 100 pm (80 kV), 160 pm (30 kV)
	TEM information limit	100 pm (200 kV), 110 pm (80 kV), 250 pm (30 kV)
Electron gun	Cold field emission gun - standard	
Aberration corrector	STEM: NEO ASCOR HOAC, TEM: CETCOR with DSS	
Corrector auto tuning system	NEO JEOL COSMO™ auto tuning system, Ad-hock tune (SIAM)	
Acceleration voltage	30 to 200 kV (30, 80, 200 kV -standard, 60, 120 kV -option)	
Magnetic field free mode	Lorentz lens settings (x50 to 80 k on screen) - standard	
Specimen movement system	X, Y and Z super fine mechanical drives, ultra fine piezo device drives - standard	
Operation type	RDS operation	



W SEM

Schottky FE-SEM

Ga FIB-SEM

Plasma FIB-SEM

X-ray micro-CT



台灣泰思肯有限公司
+886-2-2592-2777
www.tescan.com

Sales contact : Eric 廖崇光
+886-919-918-899
eric.liao@tescan.com.tw



	Single beam (SEM)		Dual beam (FIB-SEM)		Triglav™ electron column		BrightBeam™ electron column		UHR SEM
	Field-free UHR SEM		Ga ion source FIB		Orage™ Ga FIB column		iFIB+™ Xe plasma FIB column		Selective signal collection
	Low-kV resolution		Resolution		In-Beam detectors		Beam Deceleration Technology		Variable pressure (UniVac)
	Field emission gun		W thermionic emission gun		Integrated Raman spectroscopy		Unattended continuous operations		Integrated EDX analyzer
	Cross-sectioning		IC planar delayering		In-situ lamella liftout		FIB-SEM tomography		Nanoprobing
	Micro-CT systems		3D & 4D X-ray imaging		Non destructive analysis		Large-scale analysis		Fast in-situ dynamic imaging



MA·tek

The Best R&D Partner

▶ www.ma-tek.com

▶ 03-611-6678

▶ sales@ma-tek.com

閱康科技成立於2002年，自材料分析服務起家，17年來持續成長，服務項目已擴充至故障分析、可靠度驗證，為世界級的知名分析實驗室。

閱康科技擁有最尖端的測試儀器、專業的工程人員以及各產業領域的豐富經驗，目前全球共有十個實驗室，全年365天24小時提供全世界客戶最快速的分析檢測服務。

Founded in 2002, Materials Analysis Technology Inc. (MA-tek) is a leading laboratory in Materials Analysis (MA). Accompanying with the fast growing pace of business development, MA-tek has successfully expanded to provide Failure Analysis (FA) and Reliability Testing (RA) services as well, which is superior integrated service for customers in various industries. Up to now, MA-tek has set up 10 laboratories worldwide, providing around-the-clock services in logistic support and technical services.

SERVICES ITEMS



Project Based Services

- Training Courses, Lectures
- IP Strategic Planning
- Patent Infringement Study
- Benchmark Study
- Competitors Analysis
- Design Services



MA / PFA

- Decap, Delayer, Parallel Lapping
- SEM, EDX, TEM, EELS
- FIB, Circuit Editing
- SIMS, SRP, SCM, AFM
- Auger, XPS, XRD, FTIR, Raman
- Optical Profiler



EFA / ESD

- X-ray Radiography, SAT
- EMMI, InGaAs, OBIRCH
- Themos-mini, C-AFM
- Passive Volitage Contrast
- ESD, Latch-up Testing
- Wire Bonding, Packaging



Reliability Testing

- HAST, LTST, TCT, TST
- THST, PCT, UB-HAST
- HTOL, BLT, ELFR
- Reflow Test
- Device, Package Level Testing
- Board, System Level Testing

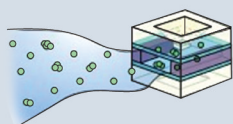


Bio Medical

- Liquid Sample TEM Service
- Bio Sample and Bio-materials EM Specimen Preparation
- Other Electron Microscopy Analysis : Liquid, Cryo, Gel, Solid, etc.
- ICP-MS, DLS, TGA, GC-MS, LC-MS

LIQUID SAMPLE TEM

閱康獨家專利開發 K-Kit 技術，為一新型液態樣品分析晶片，利用毛細現象原理實現樣品於原液態環境中獲得完整影像觀察之目的。K-kit製備樣品速度快、使用方式簡單、並且價格相對友善，是目前液態電顯市場中唯一適合應用於具複雜測試條件的學術研究、或產業相關奈米溶液分析等的創新產品，提供最精準、最直觀的液態樣品電顯影像結果。



- ▶ US 7807979 B2
- ▶ US 8969827 B2
- ▶ Anal. Chem. 2012, 84 : 6312-6316

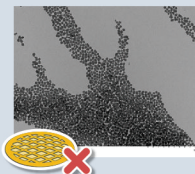


Wet

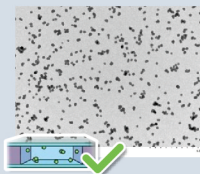


Dry

乾溼式兩用



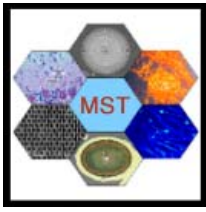
Dried on Cu grid
有粒子聚集之問題



Dried Mode of K-kit
均勻散布

目錄

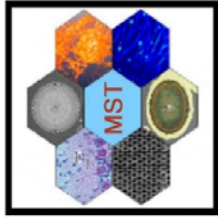
一、	第十九屆第一次台灣顯微鏡學會年會會員大會暨 第三十九屆台灣顯微鏡學會學術研討會大會議程	I
二、	第十八屆理、監事名錄	III
三、	第三十九屆台灣顯微鏡學會學術研討會 邀請演講內容摘要		
	Our recent microscopy investigations <u>Makoto Shiojiri</u> Professor Emeritus, Kyoto Institute of Technology	IV
	Senior Advisor, Faculties of Engineering and Sustainable Design, University of Toyama		
	In-situ TEM investigation of dynamic evolution in nanostructures <u>Wen-Wei Wu (吳文偉)</u>	IX
	Department of Materials Science and Engineering, National Chiao Tung University		
四、	顯微鏡技術推廣		
(I)	Highlighted features of NEOARM capabilities Mr. Noriaki Endo	1
	Assistant general manager of TEM Application Department, JEOL 捷東股份有限公司		
(II)	High-quality TEM sample preparation and 3D information Charles Lin	3
	Sr. Applications Manager, Thermo Fisher Scientific		
(III)	Introduction to AZtec family and AZtecICE Ting-Yu Wang (王廷玉)	4
	Oxford Instruments Nano Analysis Taiwan		
五、	第三十九屆台灣顯微鏡學會學術研討會 論文摘要次目錄	5
六、	攝影比賽參賽作品集目錄	52



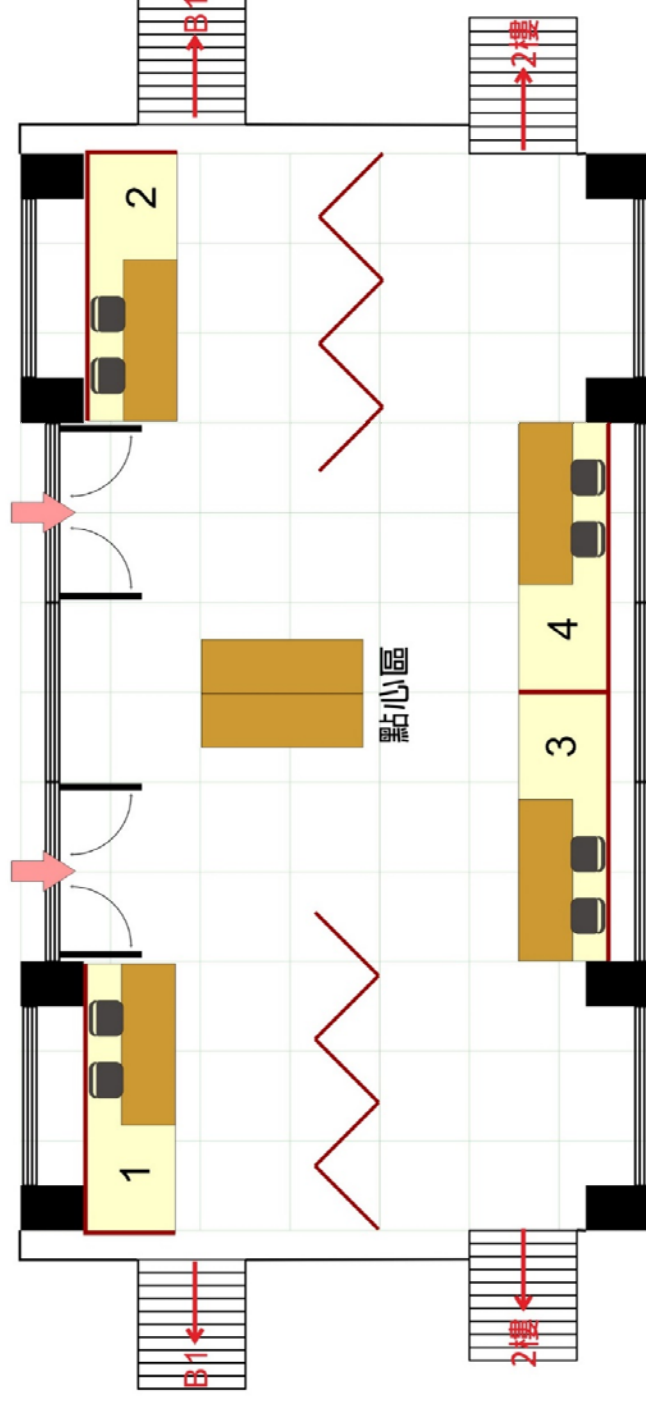
第三十九屆臺灣顯微鏡學會年會

108年9月21日(星期六) 國立臺灣大學工學院綜合大樓國際演講廳

08:30-09:30	報到
09:30-10:00	開幕
	理事長致詞與會務報告
	會員大會
10:00-11:00	<p>特邀演講(I) : Our recent microscopy investigations Dr. Makoto Shiojiri Professor Emeritus, Kyoto Institute of Technology Senior Advisor, Faculties of Engineering and Sustainable Design, University of Toyama</p>
11:00-11:30	顯微鏡技術推廣(I) : JEOL/捷東股份有限公司
11:30-12:00	<p>台灣顯微鏡學會年會會員大會 Poster Session (地點 : 一樓大廳)</p>
12:00-14:00	<p>午餐時間 (備有午餐餐盒) Poster Session (地點 : 一樓大廳)</p>
14:00-14:45	<p>特邀演講(II) : In-situ TEM investigation of dynamic evolution in nanostructures 吳文偉 特聘教授 國立交通大學 材料科學與工程學系所</p>
14:45-15:15	顯微鏡技術推廣(II) : Thermo Fisher Scientific
15:15-15:40	討論交流時間 (備有點心茶點)
15:40-16:10	顯微鏡技術推廣(III) : 牛津儀器(Oxford Instruments NanoAnalysis)
16:10-17:00	頒獎、閉幕



1. 工業技術研究院
2. 友聯光學有限公司
3. 閎康科技股份有限公司
4. 捷東股份有限公司



活動名稱：

2019/9/21 第39屆台灣顯微鏡年會

活動地點：

國立台灣大學-工學院綜合大樓 / 國際演講廳203室

台灣顯微鏡學會

第十八屆理、監事名錄

理事長 (代理)	羅聖全	工業技術研究院材料與化工研究所	博士
理事	楊哲人	台灣大學材料科學與工程學系	教授
	陳香君	台灣大學生命科學系	教授
	李志浩	清華大學工程與系統科學系	教授
	劉康庭	友聯光學股份有限公司	董事長
	謝詠芬	閎康科技股份有限公司	董事長
	薛景中	中央研究院應用科學研究中心	副研究員
	朱明文	台灣大學凝態中心	研究員
	溫政彥	台灣大學材料科學與工程學系	教授
	張立	交通大學材料科學與工程學系	教授
	蘇紘儀	台灣顯微鏡學會榮譽理事	博士
	劉全璞	成功大學材料科學與工程學系	教授
	孫啟光	台灣大學電機工程學系	教授
	簡萬能	中央研究院植物暨微生物學研究所	研究技師
	陳金富	捷東股份有限公司	總經理
	王約翰	中國醫藥大學附設醫院病理部	醫師
候補理事	陳福榮		教授
	胡宇光	中央研究院物理研究所	研究員
	孫啟光	台灣大學電機工程學系	教授
	高甫仁	陽明大學生醫光電研究所	
	鄭貽生	國立台灣大學植物科學研究所	教授
	江振誠	國家同步輻射研究中心	教授
	吳文偉	交通大學材料科學工程學系	教授
	章為皓	中央研究院化學研究所	副研究員
監事	鮑忠興	宜特科技股份有限公司	博士
	周苡嘉	國立交通大學電子物理系	教授
	曾傳銘	明志科技大學材料工程系	教授
	顏鴻威	台灣大學材料科學與工程學系	教授
	李威志	E. A. Fischione Instruments	博士
候補監事	許秋容	中興大學生命科學系	教授
	陳志遠	國立臺北科技大學智慧財產權研究所	教授

備註：王約翰理事於2019年5月17日辭去理事長一職，經2019年06月15日理監事會議通過由羅聖全理事代理理事長一職。

Invited speaker: Professor Dr. Shiojiri, Makoto



Professor Dr. Makoto Shiojiri was born in 1936 in Kyoto, Japan. He graduated from Kyoto University in 1959, and got M. Sc. from the same university in 1961, with his major in physics. After engaged in physical metallurgy at the Central Research Laboratory, Sumitomo Steel Co. Ltd., he was appointed an instructor at the Institute for Chemical Research, Kyoto University in 1962, and started his academic career, majoring in crystal and thin film physics and electron microscopy. He was conferred the D. Sc. from Kyoto University in 1967 for his studies on 'Crystallization of amorphous films prepared by vacuum-evaporation'. He was promoted to an associate professor of physics at Kyoto Institute of Technology in 1966 and was appointed a full professor of the same institute in 1975. He stayed at the Faculty of Applied and Engineering Physics of Cornell University, U.S.A. and studied the ultrahigh vacuum electron microscopy, from 1971 to 1972.

At the end of March 1999, Dr. Shiojiri retired from Kyoto Institute of Technology and is a professor emeritus of the same institute. From June 1999 to March 2007, he was with graduate school in Kanazawa Medical University as a guest professor of anatomy. Now (2014~), he is also a fellow of Faculty of Engineering, University of Toyama. In November 2015, Professor Shiojiri was awarded the Order of the Sacred Treasure, Gold Rays with Neck Ribbon, from The Emperor of Japan.

His resume is available on the website:

<http://www009.upp.so-net.ne.jp/shiojiri/top.htm>

Our recent microscopy investigations

Makoto Shiojiri

Professor Emeritus, Kyoto Institute of Technology

Senior Advisor, Faculties of Engineering and Sustainable Design, University of Toyama

1-297 Wakiyama, Kyoto 618-0091, Japan

In the 39th Annual Meeting of Microscopy Society of Taiwan (2019), I'd like to talk about the following topics which relate to our recent studies of materials science and bio science.

I. Layer Growth, Coalescence and Layer Defects of Fine η Precipitates in 7050 Aluminium Alloy:

Alloy: Recently, we have published a paper on η precipitates in 7050 Aluminium Alloy [1]. AA7050 (Al-Zn-Mg-Cu) is a heat treatable Al alloy with high toughness, strong mechanical strength, and good stress corrosion cracking resistance. It is a precipitate hardening alloy, used to build fuselage frames, wing skins and other aerospace structures. It was known that the precipitation occurs in a sequence: super-saturated solid solution \rightarrow GP zones (I and II) \rightarrow η' precipitates (4 variants) \rightarrow η precipitates (11 types, $\eta_1 - \eta_{11}$). We have found new types of η precipitates which were named η_4' and η_{12} [1]. The lecture shows high-angle annular-dark-field scanning-transmission electron microscopy (STEM) of various η precipitates, and elucidates the growth of the precipitates and the formation of layer defects in the precipitates: 1) All η type precipitates grow as hexagonal crystals whose stoichiometric composition is MgZn_2 with a stacking in Mg-base Laves phase. 2) The η - MgZn_2 precipitates nucleate and grow up laterally and layer-by-layer by the layer growth, on certain low index Al planes. 3) Both what lattice plane in the Al matrix has a 2D MgZn_2 nucleus and what lattice plane of the MgZn_2 nucleus is formed on this Al lattice would be probability events. 4) The thirteen types of η precipitates have different morphologies, shapes and habit planes. It can be generally deduced that hexagonal plates grow from the 2D nuclei that form with the basal planes of $\{0001\}_\eta$ on any of low index Al planes, while hexagonal prisms or rods grow from the 2D nuclei that form with other planes such as $\{11\bar{2}0\}_\eta$ and $\{10\bar{1}0\}_\eta$. 5) The difference of types is ascribed only to the lattice orientation relation with regard to the Al matrix. Even if new types of η precipitates find, it is not to be wondered. 6) We found a precipitate particle or twins, which formed by coalescence between two particles that developed by the layer growth and collided with each other. 7) Stacking faults were observed in

the $(11\bar{2}0)$ image of η_2 -precipitate. We deem that these stacking faults are not caused by mechanical deformation but by mis-stacking that occurs accidentally on the $\{000\bar{1}\}_\eta / \{\bar{1}11\}_{Al}$ interface in the layer growth. 8) Layer defects were observed on $\{\bar{1}100\}_\eta$ plane in the $(11\bar{2}0)_\eta$ image of η_1 -precipitate. It may be noted that structure similar to the defects is included in a unit cell of Mg_4Zn_7 crystal. We propose that these defects can be built by the coalescence or the layer growth on $\{\bar{1}100\}_\eta / \{001\}_{Al}$ interfaces. 9) We found twins with a flat coherent twin boundary along $(1\bar{2}12)_\eta$. The twins are neither caused by coalescence nor by deformation by shearing of dislocations. They are growth twins.

II. Structure and Carbonization of Green Culms of *Bambusa multiplex*: *Bambusa multiplex* (蓬萊竹) is a bamboo whose culm is straight with a height of 5~8 m and a diameter of 30~50 mm. The culm is very thick and heavy with small lumens, as represented by Japanese name ‘沈竹, a bamboo that sinks in the water’. The culms have been used for wood pulp and must be the useful material for cellulose nanofibers. Its charcoal would also be a promising new carbon material. Culms sampled and seasoned in Thailand were used in these experiments. Green culms and the charcoal carbonized from the green culms at around 700°C for 3 h in a conventional charcoal kiln were studied by means of X-ray diffraction, X-ray fluorescent element analysis, and analytical STEM [2]. It was revealed that the green culms and the charcoal contain a significant amount of Si, in particular, ~18 wt % in the skin. The green culms comprise amorphous and crystalline celluloses. The charcoal has a so-called amorphous structure which is composed of randomly distributed carbon nanotubes and fibers. The structures of Ag-doped activated charcoal powders that were produced by two different methods were also studied [2]. SEM energy dispersive X-ray spectroscopy (EDS) mapping of the green bamboo culms detected Si signals in the harder cells such as epidermis (*Ep*), cortex (*Cor*) and vascular bundle sheath (*Bs*) and between these cells [3]. The charcoal has a skin layer which originates from the *Ep* and *Cor* and the main central cylinder with many openings that originate from the expanded xylem and phloem holes. During carbonization, the Si atoms in the *Ep* and *Cor* were segregated as thin silicon oxide layers onto both the sides of the skin layer, and the Si included in the *Bs* fibers and parenchyma cells accumulated near the walls of the openings. A dynamic observation of the initial stage of carbonization was also performed *in-situ* by heating a radial longitudinal section of the bamboo

culm at a rate of 20°C/min up to 500°C [3]. Appreciable morphological change occurred in a temperature range of about 300–400°C due to the decomposition of cellulose that is the main component of the bamboo cells.

III. Nanoscale Nitride Epilayers Grown by Atomic Layer Annealing and Epitaxy at Low Temperature:

AlN-based and GaN-based materials are widely used in electronic devices such as LED. High-quality ALN and GaN epilayers are conventionally grown by metal-organic chemical vapor deposition. However, they are grown at a very high temperature (> 900°C) with a large thickness up to ~600 nm on lattice mismatched substrates such as sapphire. In the 36th Annual Meeting of MST (2016), I reported on our fabrication of InGaN/GaN LEDs with ultralow threading dislocation density and improved electronic properties [4]. Here, we show a new technique of atomic layer annealing developed to grow high-quality ultrathin AlN [5] and GaN films [6]. The atomic layer deposition is carried out together with the layer-by-layer, *in-situ* atomic layer annealing (ALA), instead of a high growth temperature for conventional MOCVD epitaxial growth. Each cycle for atomic layer epitaxy was modified with an additional step of Ar [5] or He/Ar plasma treatment [6] for ALA. Thin films prepared at 300°C by ALD without ALA have amorphous-like structure. The Ar or He/Ar plasma treatment provides sufficient crystallization energy to the surface of thin film from the incident radicals or ions at each cycle, resulting in the high crystallinity ultrathin film.

Acknowledgements: Deep thanks due all of coauthors of the references 1-6, for their friendship.

- [1] T.F. Chung, Y. L. Yang, M. Shiojiri, C. N. Hsiao, W.C. Li, C.S. Tsao, Z. Shi, J. Lin, and J.R. Yang, An atomic scale structural investigation of nanometre-sized η precipitates in the 7050 aluminium alloy. *Acta Materialia* **174**, (2019) 351-368.
- [2] V. Yordsri, C. Thanachayanont, C. Junin, M. Kawasaki, S. Asahina, T. Oikawa, A. Saiki, T. Nobuchi, and M. Shiojiri, Structural investigations on green culms and charcoal of *Bambusa multiplex*. *Microsc. Res. Tech.*, **81**, (2018) 761-769.
- [3] V.Yordsri, C. Thanachayanont, S. Asahina, Y. Yamaguchi, M. Kawasaki, T. Oikawa, T. Nobuchi, and M. Shiojiri, Scanning electron microscopy (SEM) energy dispersive X-ray spectroscopy (EDS) mapping and *in-situ* observation of carbonization of culms of *Bambusa multiplex*. *Microsc. Microanal.* **24**, (2018) 156-162.

- [4] H.Y. Shih, M. Shiojiri, C.H. Chen, S.F. Yu, C.T. Ko, J.R. Yang, R.M. Lin, and M.J. Chen, Ultralow threading dislocation density in GaN epilayer on near-strain-free GaN compliant buffer layer and its applications in hetero-epitaxial LEDs. *Sci. Rep.* **5**, (2015) Article number 13671.
- [5] H.Y. Shih, W.H. Lee, W.C. Kao, Y.C. Chuang, R.M. Lin, H.C. Lin, M. Shiojiri, and M.J. Chen, Low-temperature atomic layer epitaxy of AlN ultrathin films by layer-by-layer, *in-situ* atomic layer annealing. *Sci. Rep.* **7**, (2017) Article number:39717.
- [6] W.H. Lee, Y.T. Yin, P.H. Cheng, J.J. Shyue, M. Shiojiri, H.C. Lin, and M.J. Chen, Nanoscale GaN epilayer grown by atomic layer annealing and epitaxy at low temperature. *ACS Sustainable Chem. Eng.* **7**, (2019) 487-495.

Invited speaker: Professor Dr. Wen-Wei Wu 吳文偉教授

現職：國立交通大學材料科學與工程學系特聘教授

學歷：國立清華大學材料科學與工程所博士, 2003

經歷：

國立交通大學材料科學與工程學系教授, 2014

國立交通大學材料科學與工程學系副教授, 2011~2014

國立交通大學材料科學與工程學系助理教授,

2008~2011

國立清華大學材料科學與工程學系 博士後研究員,

2003~2008

專長：電子顯微鏡、半導體材料、奈米光電材料、微

電子材料與製程、材料顯微結構及缺陷分析、薄膜工程

簡介：吳文偉教授，國立清華大學材料科學與工程博士畢業(2003)，2008年2月起任教於國立交通大學材料科學與工程學系。吳文偉教授研究領域為電子顯微鏡、半導體材料、奈米光電材料、微電子材料與製程。2008年與研究團隊發現銅晶體內部之奈米雙晶結構與晶界接合處可有效遲滯銅原子的電致遷移現象，對於積體電路製程技術的開發極具啟發作用，成果獲刊於國際頂尖期刊《Science》；隔年獲頒發「2009年中央研究院年輕學者研究著作獎」。2014以「電阻式記憶體中傳導奈米燈絲之演變研究」獲得「第十二屆有庠科技奈米科技類論文獎」，為世界上首次成功用材料分析方法直接觀察電阻式記憶體透過氧化還原而導致電阻值轉換(switching)及結構動態變化完整過程的論文，對元件操作與物理模型提供良好的材料分析方法與驗證機制。此外，吳教授也榮獲「103年度科技部吳大猷先生紀念獎」、「中國電機工程師學會優秀青年電機工程師獎」、「台灣真空學會年輕學者獎」、「台灣電子材料與元件協會傑出青年獎」以及「中國材料學會傑出年輕學者獎」等研究獎勵。吳教授專長為臨場穿透式電子顯微鏡研究，針對材料在通電、加熱、以及液態的環境下的物理現象與結構演變及成長動力學有許多創新與突破性的研究成果發表於頂尖期刊，獲得極大的迴響，因此更於107年榮獲「中國電機工程師學會傑出電機工程教授獎」以及「科技部傑出研究獎」。



***In-situ* TEM investigation of dynamic evolution in nanostructures**

Wen-Wei Wu (吳文偉)

**Department of Materials Science and Engineering, National Chiao Tung University,
Hsinchu 300, Taiwan, ROC**

In-situ TEM is a technique that allows a direct observation of dynamic properties in nanoscale. In situ investigation of the temperature induced phase transformation, structural and chemical evolution of nanocrystals is important for understanding the structure and stability of nanomaterials. As the technology advances, the scaling issue of nanodevices has attracted wide consideration, especially the exploration of atomic-scale structural dynamics. The appropriate utilization of the *in-situ* TEM will be beneficial in studying the fundamental mechanisms of dynamic reactions, switching behaviors and electrical properties of nanodevices. Therefore, we use *in-situ* TEM for direct observation of the dynamic evolution in nanomaterials and nanodevices, which is important for understanding their mechanisms and aiding to the practical aspect. Here, we present the most recent progress in observing dynamic processes in nanoscale by *in-situ* TEM.

Highlighted features of NEOARM capabilities

Noriaki Endo*, Hiroki Hashiguchi, Ichiro Ohnishi, and Eiji Okunishi

JEOL Ltd., Akishima, Tokyo, Japan

*nendo@jeol.co.jp

Recently, there has been an increase in the need for various forms of high-resolution imaging of materials containing light elements and of specimens susceptible to electron beam irradiation damage. The demands for aberration-corrected STEM/TEMs with simplified operation are also increasing. Therefore, we have developed the NEOARM atomic-resolution analytical electron microscope to meet these various needs.

The NEOARM is equipped with JEOL's unique Cold-FEG and a new Cs corrector (ASCOR) that compensates for higher-order aberrations. The combination of Cold-FEG and ASCOR enables atomic-resolution imaging at not only an accelerating voltage of 200 kV but also at low voltages such as 30 kV. Figure 1 shows a HAADF-STEM image of GaN [211] obtained at 200 kV using an ultra-high-resolution pole piece. We observed the dumbbell structure with a 63 pm spacing clearly. Moreover, higher-resolution reflections, such as -546 and -555, can also be seen in the FFT pattern.

This microscope is also equipped with an automated aberration correction system, JEOL COSMO™, which has adopted a new aberration correction algorithm. Therefore, no special sample is required for aberration correction, leading to high precision and quick correction of higher-order aberrations up to the fifth order. This new system enables faster processing than the conventional correction algorithm, automating corrector alignment and thereby eliminating the complicated tuning of the corrector. These features enable high-throughput atomic-resolution imaging and analysis, even at low accelerating voltages, for all levels of users.

This year, we added a wide-gap pole piece coupled with a 158 mm² Dual SDD. The solid angle is now better than 2.2 sr. Figure 2 shows atomic-resolution EDS column maps of SrTiO₃ acquired within 300 seconds. Note the clarity of the oxygen column map.

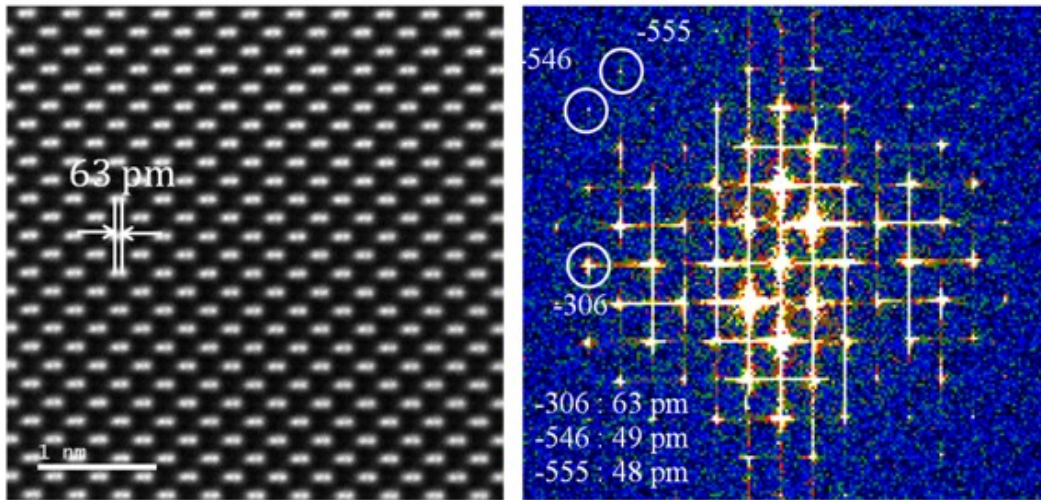


Figure 1. HAADF-STEM image of GaN [211] and its FFT pattern.

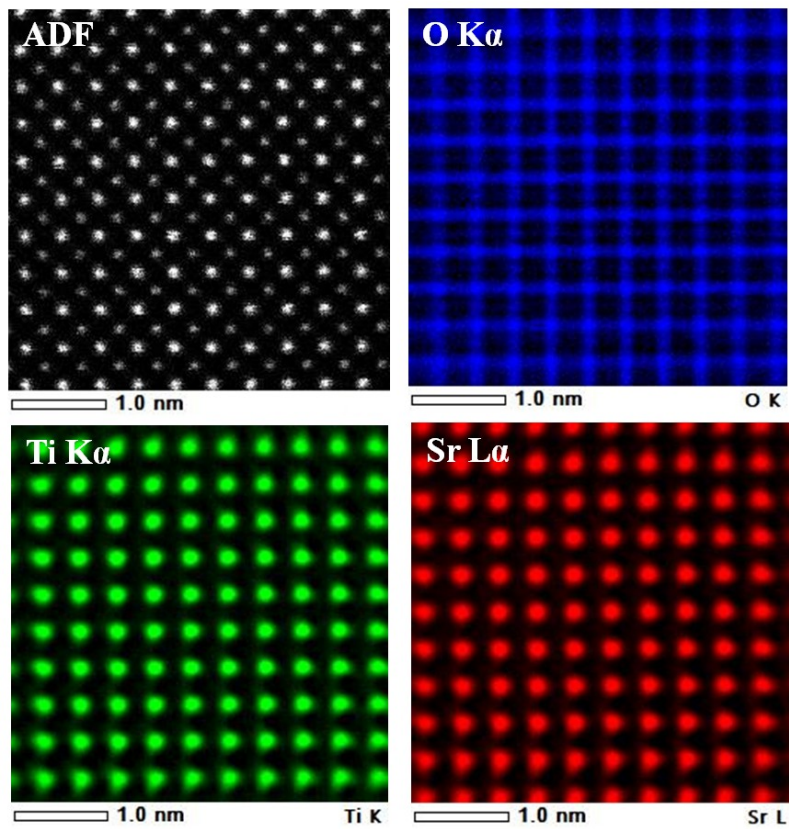


Figure 2. EDS column maps of SrTiO₃.

Scios 2 DualBeam System

The most versatile high-performance DualBeam instrument

The Scios 2 DualBeam System delivers best-in-class performance in sample preparation, subsurface and 3D characterization for the widest variety of samples.

The Thermo Scientific™ Scios™ 2 DualBeam™ System is an ultra-high-resolution analytical system that provides outstanding sample preparation and 3D characterization performance for the widest range of samples, including magnetic and nonconductive materials. With innovative features designed to increase throughput, precision, and ease of use, the Scios 2 DualBeam System is an ideal solution to meet the needs of scientists and engineers in advanced research and analysis across academic, government and industrial research environments.

High-quality TEM sample preparation

Scientists and engineers constantly face new challenges that require highly localized characterization of increasingly complex samples with ever smaller features. The latest technological innovations of the Scios 2 DualBeam System, in combination with the easiest-to-use, most comprehensive Thermo Scientific AutoTEM™ 4 Software (optional) and our application expertise, allow for fast and easy preparation of site-specific HR-S/TEM samples for a wide range of materials. In order to achieve the high-quality results, final polishing with low-energy ions is required to minimize surface damage on the sample. The Thermo Scientific Sidewinder™ HT Focused Ion Beam (FIB) column not only delivers high-resolution imaging and milling at high voltages, but has also good low-voltage performance, enabling the creation of high-quality TEM lamella.

High-quality subsurface and 3D information

Subsurface or three-dimensional characterization is often required to better understand the structure and properties of a sample. The Scios 2 DualBeam System with optional Thermo Scientific Auto Slice & View™ 4 (AS&V4) Software allows for high-quality, fully automated acquisition of multi-modal 3D datasets, including, among others, BSE imaging for maximum materials contrast, Energy Dispersive Spectroscopy (EDS) for compositional information, and Electron Backscatter Diffraction (EBSD) for microstructural and crystallographic information. Combined with Thermo Scientific Avizo™ Software, it delivers a unique workflow solution for high-resolution, advanced 3D characterization and analysis at the nanometer scale.

Key benefits

Fast and easy preparation of high-quality, site-specific, TEM and atom probe samples using the Sidewinder HT ion column

Ultra-high resolution imaging using the Thermo Scientific NiCoI™ electron column with best-in-class performance on the widest range of samples, including magnetic and non-conductive materials

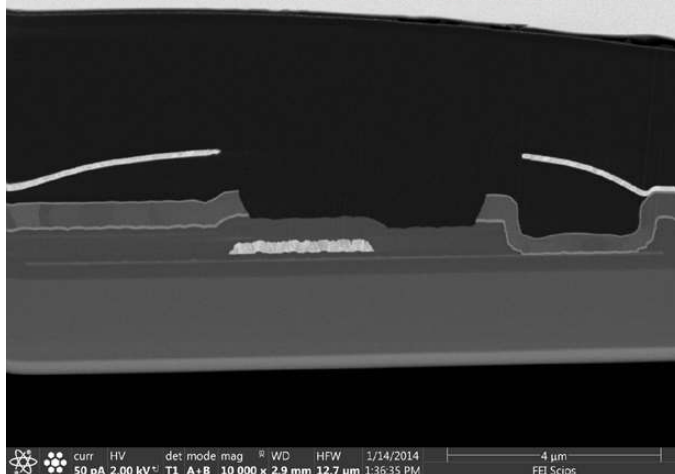
The most complete sample information with sharp, refined, and charge-free contrast obtained from a variety of integrated in-column and below-the-lens detectors

Access the high quality, multi-modal subsurface and 3D information with precise targeting of the region of interest using optional AS&V4 Software

Precise sample navigation tailored to individual application needs thanks to the high flexibility 110 mm stage and in-chamber Thermo Scientific Nav-Cam™ Camera

Artifact-free imaging and patterning with dedicated modes such as DCFI, Drift Suppression and Thermo Scientific SmartScan™ Modes

Optimize your solution to meet specific application requirements thanks to flexible DualBeam configuration



Introduction to AZtec family and AZtecICE

Ting-Yu Wang (王廷玉)

Oxford Instruments Nano Analysis Taiwan

AZtec is the EDS and EBSD data acquisition and data processing software of Oxford Instruments Nano Analysis. For EDS analysis, it not only provides routine SEM and TEM EDS analysis but also some powerful solution like AZtecFeature, AZtecLayerprobe etc. For EBSD analysis, data acquisition is easy and straightforward. With version change in last two years, it now can provides more intuitive result after data acquisition. We now announced a new EBSD data processing software – AZtecICE. It's much more easy to learn but keep flexibility for expert users, and also it comes with new functions compare with Channel 5.

Semiconductor analysis

Integrated solutions from failure analysis to a full characterisation in the electron microscope

EBIC & EBAC
LIFTOUT
EDS
WDS
EBSD



Better insights and increased productivity

OXFORD
INSTRUMENTS

The Business of Science®

第三十九屆臺灣顯微鏡學會年會研討會

論文摘要

<p>A-01</p>	<p>Interactions in between the variant-pair of η precipitates in the Al-Zn-Mg-Cu aluminum alloy Tsai-Fu Chung (鍾采甫)¹, Yo-Lun Yang (楊侑倫)², Makoto Shiojiri^{3*}, Chien-Nan Hsiao (蕭健男)⁴, Wei-Chih Li (李威志)⁵, Jer-Ren Yang (楊哲人)^{1*} ¹ Department of Materials Science and Engineering, National Taiwan University, Taipei, Taiwan. ² Department of Mechanical Engineering, Imperial College London, London SW7 2AZ, UK. ³ Kyoto Institute of Technology, Kyoto 606-8585, Japan. ⁴ Taiwan Instrument Research Institute, Hsinchu, Taiwan. ⁵ E.A. Fischione Instruments, Inc., 9003 Corporate Circle, Export, PA 15632, U.S.A.</p>	<p>11</p>
<p>A-02</p>	<p>Atomic Layer Deposition System with Plasma Etching Yu-Ting Peng(彭裕庭),* Yu-Lun Liu(劉宇倫), Chin-Ying Chou(周晶瑩), Chien-Chun Chen(陳健群) Department of Engineering and System Science, National Tsing Hua University</p>	<p>12</p>
<p>A-03</p>	<p>Transmission Electron Microscopy Specimen Preparation by Focused Ion Beam System Yu-Lun Liu (劉宇倫), * Yu-Ting Peng(彭裕庭), Chin-Ying Chou(周晶瑩), and Chien-Chun Chen(陳健群) Department of Engineering and System Science, National Tsing Hua University, Hsinchu, Taiwan</p>	<p>13</p>
<p>A-04</p>	<p>The interaction of T_1 and θ' precipitates with respect to dislocations in the AA2050 aluminium alloy Tsai-Fu Chung (鍾采甫)¹, Yo-Lun Yang (楊侑倫)², Makoto Shiojiri^{3*}, Chien-Nan Hsiao (蕭健男)⁴, Wei-Chih Li (李威志)⁵, Jer-Ren Yang (楊哲人)^{1*} ¹ Department of Materials Science and Engineering, National Taiwan University, Taipei, Taiwan. ² Department of Mechanical Engineering, Imperial College London, London SW7 2AZ, UK. ³ Kyoto Institute of Technology, Kyoto 606-8585, Japan. ⁴ Taiwan Instrument Research Institute, Hsinchu, Taiwan. ⁵ E.A. Fischione Instruments, Inc., 9003 Corporate Circle, Export, PA 15632, U.S.A</p>	<p>14</p>

A-05	Annealing-induced abnormal hardening in a cold rolled CoCrNi medium entropy alloy Shih-Yu Chen (陳思妤)*, and Jer-Ren Yang (楊哲人) Department of Materials Science and Engineering, National Taiwan University, Taipei, Taiwan	15
A-06	A Novel Denoising Technique by Using Machine Learning Based Approach Ren-Fong Cai (蔡任豐)*, Mu-Tung Chang (張睦東), and Shen-Chuan Lo (羅聖全) Material and Chemical Research Laboratories, Industrial Technology Research Institute, Hsinchu, Taiwan	16
A-07	The Application of K-means Clustering to EELS Mapping Ren-Fong Cai (蔡任豐)*, Mu-Tung Chang (張睦東), and Shen-Chuan Lo (羅聖全) Material and Chemical Research Laboratories, Industrial Technology Research Institute, Hsinchu, Taiwan	18
A-08	Influence of tempering treatment on mechanical properties and the hydrogen embrittlement of NiCrMo steel Shih-Chieh Kao (高士傑), and Hsin-Chih Lin(林新智) Department of Materials Science and Engineering, National Taiwan University, Taipei, Taiwan	19
A-09	Precipitation Behavior in Custom 475 Maraging Stainless Steel Cheng-Yao Huang(黃正堯)*, and Hung-Wei Yen (顏鴻威) Department of Materials Science and Engineering, National Taiwan University, Taipei, Taiwan	20
A-10	Study on the effects of Nb-Ta-Ti-V-Zr high entropy alloys composition and roughness on bone-forming cells Wei Yu (游薇) ¹ , Su-Jien Lin (林世傑) ² , and Yi-Chia Chou (周苡嘉) ^{1*} ¹ Electrophysics, National Chiao Tung University, Hsinchu, Taiwan Hsinchu, Taiwan ² Department of Orthopaedic Surgery, Chang Gung Memorial Hospital, Linkou, Taoyuan County 33305, Taiwan	21
A-11	TEM Analysis of structural defects in homoepitaxial (111) diamond film on nickel-coated HPHP diamond Kun-An Chiu (丘坤安)*, Wei-Lin Wang (王尉霖), Thi Hien Do (杜氏賢), and Li Chang (張立) Department of Materials Science and Engineering, National Chiao Tung University, Hsinchu, Taiwan	22

A-12	<p>Study on the Effects of Different Mn Contents on Annealing and Mechanical Twinning of CoCrFeMn_xNi (X=0~1) High Entropy Alloy</p> <p>Po-Han Chiu(邱柏翰),* and Jer-Ren Yang(楊哲人)</p> <p>Department of Materials Science and Engineering, National Taiwan University, Taipei, Taiwan</p>	23
A-13	<p>Study on Annealing Twins of Co-Cr-Fe-Mn-Ni High Entropy Alloy</p> <p>Ching-Chien Chen*(陳敬謙), Po-Han Chiu(邱柏翰), and Jer-Ren Yang(楊哲人)</p> <p>Department of Materials Science and Engineering, National Taiwan University, Taipei, Taiwan</p>	24
A-14	<p>Observing the growth and distribution of annealing twins at low annealing temperature in FeCoNiCr high entropy alloy</p> <p>Yo-Shiuan Lin (林佑諠)*, and Jer-Ren Yang (楊哲人)</p> <p>Department of Materials Science and Engineering, National Taiwan University, Taipei, Taiwan</p>	25
A-15	<p>The Effect of Two-step Heat Treatment on the Carbide-free Bainite</p> <p>Ting-Mu Chung (莊庭牧)¹, Yu-Ting Tsai(蔡宇庭)², Yu-Wei Lai(賴昱維)^{1*}, Jer-Ren Yang(楊哲人)¹</p> <p>¹Department of Materials Science and Engineering, National Taiwan University, Taipei, Taiwan ² China Steel Cooperation, Kaohsiung, Taiwan</p>	26
A-16	<p>The influence of low temperature on the hydrogen embrittlement of NiCrMo steel</p> <p>Li-Jen Ho(何立仁), Chih-Fu Tu(涂植夫), Hsin-Chih Lin(林新智)</p> <p>Department of Materials Science and Engineering, National Taiwan University, Taipei, Taiwan</p>	27
A-17	<p>Mechanical Property and Microstructure of Cryogenic Temperature and High-strain-rate Compressive Deformation in the FeCoNiCrMn High-entropy Alloy</p> <p>Pin-Jung Chem(陳品戎)*, Jen-Ren Yang(楊哲人)</p> <p>Department of Materials Science and Engineering, National Taiwan University, Taipei, Taiwan</p>	28
A-18	<p>Auto-tempered martensite and interpenetrating twin in lath martensite</p> <p>Tzu-Ching tsao (曹梓敬), * and Jer-Ren Yang (楊哲人)</p> <p>Department of Materials Science and Engineering, National Taiwan University, Taipei, Taiwan</p>	30
A-19	<p>Investigation of Strain-induced Precipitation Behavior of Niobium Micro-alloyed Steels at High Temperature</p> <p>Tzu-Ching tsao (曹梓敬), * and Jer-Ren Yang (楊哲人)</p> <p>Department of Materials Science and Engineering, National Taiwan University, Taipei, Taiwan</p>	31

A-20	<p>Study of Self-Propagating Reaction in the Ni/amorphous-Si Reactive Multilayers</p> <p>Heng Lam Kam (甘慶霖), Yuan-Wei Chang (張元蔚), Wen-Hsien Hsu (徐文賢), Chien Chang (張阡), and Yi-Chia Chou (周苡嘉)*</p> <p>Electrophysics, National Chiao Tung University, Hsinchu, Taiwan (R.O.C.)</p>	32
A-21	<p>Morphology Changes of MoS₂ Nanosheets during Electrochemical Reactions in Li-ion Batteries</p> <p>Chuan-Yu Wei(魏川育),* Pei-Chin Lee(李珮勤), Chin-Wei Tsao(曹晉璋), Lan-Hsuan Lee(李藍暄), and Cheng-Yen Wen(溫政彥)</p> <p>Department of Materials Science and Engineering, National Taiwan University, Taipei, Taiwan</p>	33
A-22	<p>Chemical deviation of thermodynamic equilibrium under dynamic strain-induced austenite reversion in Mn-rich steel</p> <p>Guan-Ju Cheng(程冠儒),^a Lola Lilensten^b, Ching-Yuan Huang^c, Dierk Rabbe, Baptiste Gault^{b,*}, and Hung-Wei Yen (顏鴻威)^{a*}</p> <p>^a Department of Materials Science and Engineering, National Taiwan University, Taipei, Taiwan ^b Department of Microstructure Physics and Alloy Design, Max-Planck-Institut für Eisenforschung GmbH, Düsseldorf, Germany ^c Iron and Steel R&D Department, China Steel Corporation, Chung Kang Road, Kaohsiung, Republic of China</p>	35
A-23	<p>Observation of SiGe Nanodots Produced by Thermal Oxidation of SiGe Thin Film</p> <p>Yu-Tao Sun(孫宇韜),* and Cheng-Yen Wen(溫政彥)</p> <p>Department of Materials Science and Engineering, National Taiwan University, Taipei, Taiwan</p>	36
A-24	<p>Study on Microalloyed Medium-Manganese Steels in Quenching and Austenite Reversion Process</p> <p>Shan-Chun Yang (楊善淳),* and Hung-Wei Yen (顏鴻威)</p> <p>Department of Materials Science and Engineering, National Taiwan University, Taipei, Taiwan</p>	37
A-25	<p>Graphene Window for Scanning Electron Microscopy of Liquid</p> <p>Yu-Yu Chen(陳昱宇),* and Cheng-Yen Wen(溫政彥)</p> <p>Department of Materials Science and Engineering, National Taiwan University, Taipei, Taiwan</p>	38
A-26	<p>Using Transmission Electron Microscope to Analyze the Stacking Form of Graphene Grown in Chemical Vapor Deposition</p> <p>I-Ta Wang(汪奕達),* and Cheng-Yen Wen(溫政彥)</p> <p>Molecule Science and Technology Program, National Taiwan University, Taipei, Taiwan</p>	39

A-27	<p>An Investigation of Different Ageing Treatments in AA7050 Al Alloys Yo-Ming Pua* (潘有銘), Tsai-Fu Chung(鍾采甫), and Jer-Ren Yang(楊哲人) Department of Materials Science and Engineering, National Taiwan University, Taipei, Taiwan</p>	40
A-28	<p>Ferromagnetic Hollow Micro-spheres Composite and its SERS Application Pei-Kai Hsu,^{1,*} Yu-Fang Huang,^{1,2} Wen-Chi Huang,¹ Shih-Yun Chen,¹ Jenn-Ming Song,³ Alexandre Gloter,⁴ ¹ Department of Materials Science and Engineering, National Taiwan University of Science and Technology, Taipei, Taiwan ² Material and Chemical Research Laboratories, Industrial Technology Research Institute, Hsinchu, Taiwan ³ Department of Materials Science and Engineering, National Chung Hsing University, Taichung, Taiwan ⁴ Laboratoire de Physique des Solides, Université Paris Sud, CNRS UMR 8502, F-91405 Orsay, France</p>	41
A-29	<p>Reliability of EDS Line Profiles Extracted from Spectrum Images Jong-Shing Bow(鮑忠興)^{1*}, Darry Chen(陳緯綺)¹, Yu-Feng Ko(葛裕逢)¹, Chien-Nan Hsiao (蕭健男)² ¹ Integrated Service Technology, Hsinchu, Taiwan, R.O.C ² Taiwan Instrument Research Center, National Applied Research Laboratories, Taiwan</p>	42
A-30	<p>Recently Progress of Lithium Ion Battery Related Environmental Stages Development in ITRI Shih-Yi Liu (劉鈺誼), Yu-Fang Haung (黃鈺方), Chun-Wei Haung (黃浚璋), and Shen-Chuan Lo (羅聖全)* Material and Chemical Research Laboratories, Industrial Technology Research Institute, Hsinchu, Taiwan</p>	43
A-31	<p>免疫電鏡對豬流行性下痢病毒結構探討 Yu-Hsiang Chen(陳育祥)^{1,3*}, Hsiang-Ching Wang(王翔靖)², Shen-Chuan Lo (羅聖全)¹ and Hsin-Lung Chen(陳信龍)³ ¹ Material and Chemical Research Laboratories, Industrial Technology Research Institute, Hsinchu, Taiwan ² Biomedical Technology and Device Research Laboratories, Industrial Technology Research Institute, Hsinchu, Taiwan. ³ Department of Chemical Engineering, National Tsing Hua University, Hsinchu, Taiwan.</p>	45

A-32	<p>EPMA study on the oxidized Tb_xDy_{1-x}Fe_{2-y} thin films: influence of thermal annealing on the segregation of Fe nanocluster from the oxide compositions</p> <p>Chih-Hao Lee (李志浩)*, Wen-Ching Chang(張文青) and Aswin Kumar Anbalagan</p> <p>Department of Engineering and System Science, National Tsing Hua University</p>	46
A-33	<p>Plasmonic performance and SERS effect of meso-hollow CeO₂ spheres with Ag nanoparticles deposited</p> <p>Yi-Che Chen,¹ Eric Nestor Tseng,¹ Yin-Ting Hsiao,¹ Shih-Yun Chen,^{1*} Alexandre Gloter² and Jenn-Ming Song³</p> <p>¹ Department of Materials Science and Engineering, National Taiwan University of Science and Technology, Taipei, Taiwan.</p> <p>² Laboratoire de Physique des Solides, Université Paris Sud, CNRS UMR 8502, F-91405 Orsay, France.</p> <p>³ Department of Materials Science and Engineering, National Chung Hsing University, Taichung 402, Taiwan.</p>	47
A-34	<p>Stoichiometric microscopy based on XANES and EELS for phase change nanomaterials</p> <p>Ling Lee (李寧), Tze-Yi Yang(楊子逸), and Yu-Lun Chueh (闕郁倫)*</p> <p>Department of Materials Science and Engineering, National Tsing Hua University, Hsinchu, Taiwan</p>	48
A-35	<p>Epochal high-performance aluminium-ion batteries based on three-dimensional molybdenum diselenide helical nanorod arrays</p> <p>Tzu-Yi Yang, Shu-Chi Wu and Yu-Lun Chueh*</p> <p>Department of Materials Science and Engineering, National Tsing-Hua University, Hsinchu, Taiwan, Republic of China</p>	49
A-36	<p>Epitaxial growth of zirconium nitride grown on Si substrate by reactive magnetron sputtering</p> <p>Thi-Hien Do (杜氏賢)*, Yih-Yang Tseng (曾奕洋), Kun-An Chiu (丘坤安), and Li Chang (張立)</p> <p>Department of Materials Science and Engineering, National Chiao Tung University, Hsinchu, Taiwan</p>	50
A-37	<p>Study of annealing twin on CoCrFeMnNi high-entropy alloy</p> <p>Tulustia Japanesa¹, Shao-Pu, Tsai², Pin-Jung, Chen², Akhmad A. Korda¹, Jer-Ren, Yang²</p> <p>¹ Department of Metallurgical Engineering, Bandung Institute of Technology, Indonesia</p> <p>² Department of Materials Science and Engineering, National Taiwan University, Taiwan</p>	51

Interactions in between the variant-pair of η precipitates in the Al-Zn-Mg-Cu aluminium alloy

Tsai-Fu Chung¹, Yo-Lun Yang², Makoto Shiojiri^{3**}, Chien-Nan Hsiao⁴, Wei-Chih Li⁵,
Jer-Ren Yang^{1,*}

¹ Department of Materials Science and Engineering, National Taiwan University, Taipei, Taiwan.

² Department of Mechanical Engineering, Imperial College London, London SW7 2AZ, UK.

³ Kyoto Institute of Technology, Kyoto 606-8585, Japan.

⁴ Taiwan Instrument Research Institute, Hsinchu, Taiwan.

⁵ E.A. Fischione Instruments, Inc., 9003 Corporate Circle, Export, PA 15632, U.S.A.

For Al-Zn-Mg-Cu aluminium alloys, 13 types of η precipitates would possess the symmetrically variants distributed on the closed plane of the Al matrix parallel to the $\{0001\}_\eta$, $\{2\bar{1}\bar{1}0\}_\eta$, or $\{10\bar{1}0\}_\eta$ interfaces of precipitates [1]. It was reported that the η_2 precipitates, growing on the $(1\bar{1}\bar{1})_{Al} // (0001)_{\eta_2}$ habit plane where the growth direction follows with $[110]_{Al} // [10\bar{1}0]_{\eta_2}$, would own four equivalent variants on $\{1\bar{1}\bar{1}\}_{Al}$, i.e., $\eta_2^{(1)}$ to $\eta_2^{(4)}$ variants [2]. Whether the interactions would occur in between these four equivalent variants of η_2 during the growth of precipitates has yet to be elucidated. In the present work, along the $[110]_{Al}$ zone axis, the atomic arrays of the interfacial areas in between $\eta_2^{(1)}$ and $\eta_2^{(2)}$ respectively grown on $(1\bar{1}\bar{1})_{Al}$ and $(1\bar{1}1)_{Al}$ planes shows that the nearly-twinning relationship has been resolved. On the other hand, along the $[\bar{1}\bar{1}0]_{Al}$ zone axis, it also reveals nearly-twinning configuration in between the variant-pair of η_2 .

References

[1] T.-F. Chung, et al., *Acta Mater.* 174 (2019) 351-368.

[2] T.-F. Chung, et al., *Acta Mater.* 149 (2018) 377-387.

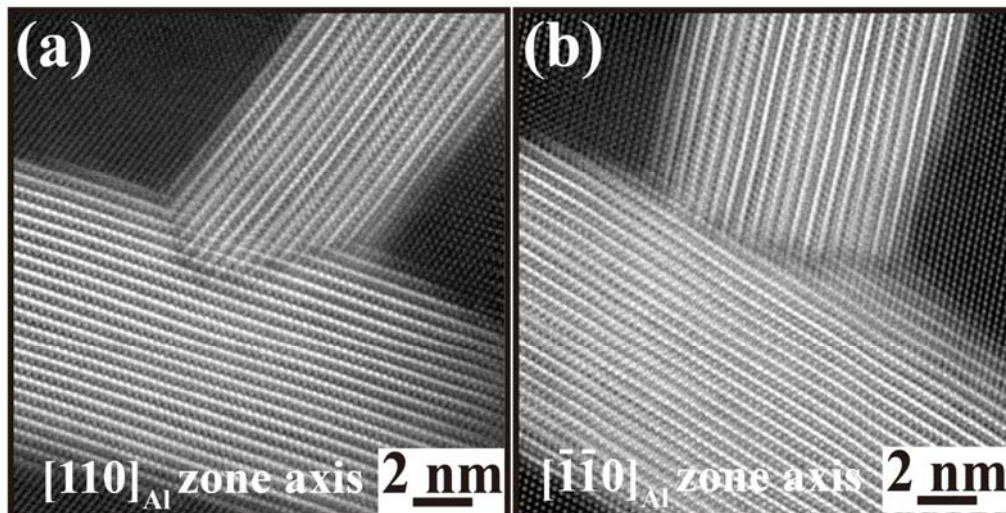


Figure 1. HAADF-STEM images, along the zone axes of $[110]_{Al}$ and $[\bar{1}\bar{1}0]_{Al}$, showing Nearly-twinning configuration in between the variant-pair of η_2 .

Atomic Layer Deposition System with Plasma Etching

Yu-Ting Peng(彭裕庭),^{1*} Yu-Lun Liu(劉宇倫),¹ Chin-Ying Chou(周晶瑩),¹
Chien-Chun Chen(陳健群)¹

¹ Department of Engineering and System Science, National Tsing Hua University
*trevorpeng9654@gmail.com

The thin film of Al₂O₃ was used to protect the surface of the substrate from deposited impurities. To coat a high-quality protective film on the surface, atomic layer deposition (ALD) is a promising method. Unlike the traditional processes, we built our own ALD system with inductively coupled plasma (ICP) that can generate cleaner samples under the protective film. Before depositing the Al₂O₃ thin film, we used ICP first to clean the substrate surface preventing impurities from being covered below the film. In this study, we depict the scanning transmission electron microscope (STEM) images of samples with and without ICP cleaning, respectively. From those results, one can observe that the ICP-cleaned samples provide STEM image of higher contrast.

Transmission Electron Microscopy Specimen Preparation by Focused Ion Beam System

Yu-Lun Liu (劉宇倫),^{1*} Yu-Ting Peng(彭裕庭),¹ Chin-Ying Chou(周晶瑩),¹ and
Chien-Chun Chen(陳健群)¹

¹ Department of Engineering and System Science, National Tsing Hua University, Hsinchu,
Taiwan

*kc25566@gmail.com

In recent years, focused ion beam (FIB) has been widely used in the field of materials science. By controlling the energy and intensity of the ion beam carefully, we can use FIB to perform precise nanomachining. One of the important applications of FIB is the preparation of transmission electron microscopy (TEM) specimen. Unlike the traditional preparation procedure that is time consuming and complicated, we provide a better method of TEM specimen preparation by the milling and lift-out technique of FIB. In this poster, the TEM specimen preparation procedures by a dual-beam FIB and the corresponding scanning electron microscopy (SEM) images will be presented.

References

1. L. A. Giannuzzi and F. A. Stevie, *Micron*, **197-204** (1999).

The interaction of T_1 and θ' precipitates with respect to dislocations in the AA2050 aluminium alloy

Tsai-Fu Chung¹, Yo-Lun Yang², Makoto Shiojiri^{3**}, Chien-Nan Hsiao⁴, Wei-Chih Li⁵, Jer-Ren Yang^{1,*}

¹ Department of Materials Science and Engineering, National Taiwan University, Taipei, Taiwan.

² Department of Mechanical Engineering, Imperial College London, London SW7 2AZ, UK.

³ Kyoto Institute of Technology, Kyoto 606-8585, Japan.

⁴ Taiwan Instrument Research Institute, Hsinchu, Taiwan.

⁵ E.A. Fischione Instruments, Inc., 9003 Corporate Circle, Export, PA 15632, U.S.A.

近年來，於既有 2 系列鋁銅(Al-Cu)合金中，添加微量鋰(Li)元素，卻意外提升機械強度。除此之外，由於 Li 元素特性，因而大幅減少鋁合金重量。而符合我國前瞻性綠能材料之方針。高強度的 AA2050 (Al-Cu-Li)鋁合金其奈米等級 T_1 (Al₂CuLi)與 θ' (Al₂Cu)析出物為主要提供強度貢獻主因，但微觀角度而言，此兩類析出物與差排交互作用為 Bowing 或 Cutting 機制之情況尚未明瞭。本研究藉由奈米壓痕儀(Nano-indenter)與變形式-動態穿透式電子顯微鏡(deformed in-situ TEM)探討其對應之應力-深度位移曲線，而細部了解析出對差排交互作用情況。再配合球面像差校正高解度掃描穿透式電子顯微鏡(Cs-corrected HAADF-STEM)於不同晶帶軸(zone axis)證實移動中的差排切過 T_1 與 θ' 析出物(即，Cutting 機制)而造成析出物其內部原子排列產生變化，進一步深耕此交互作用對機械性能之影響。

關鍵字: AA2050 (Al-Cu-Li)鋁合金, T_1 (Al₂CuLi)與 θ' (Al₂Cu)析出物, Cs-corrected HAADF-STEM

Annealing-induced abnormal hardening in a cold rolled CoCrNi medium entropy alloy

Shih-Yu Chen (陳思妤)*, and Jer-Ren Yang (楊哲人)

Department of Materials Science and Engineering, National Taiwan University, Taipei, Taiwan

* r07527031@ntu.edu.tw

A CoCrNi equiatomic medium entropy alloy (MEA) with a single solid solution was cold rolled with a thickness reduction of ~70% at room temperature, followed by annealing treatment with relative low temperature. Annealing-induced abnormal hardening was observed for cold rolled alloy after annealing treatment at 873 K. Detailed microstructural characterizations indicated that the abnormal hardening phenomenon is not due to the precipitation hardening or nanocrystalline. A similar phenomenon was found in severe plastic deformation (SPD) in CrCoMnFeNi and CoCrNi after annealing. Although the main reason of abnormal hardening in CoCrNi is still unclear, further research will be continued by EBSD (Electrical Backscatter Diffraction) and TEM (Transmission Electron Microscopy).

References

1. Gu, J., & Song, M. (2019).
2. Schuh, B., Mendez-Martin, F., Völker, B., George, E. P., Clemens, H., Pippan, R., & Hohenwarter, A. (2015).

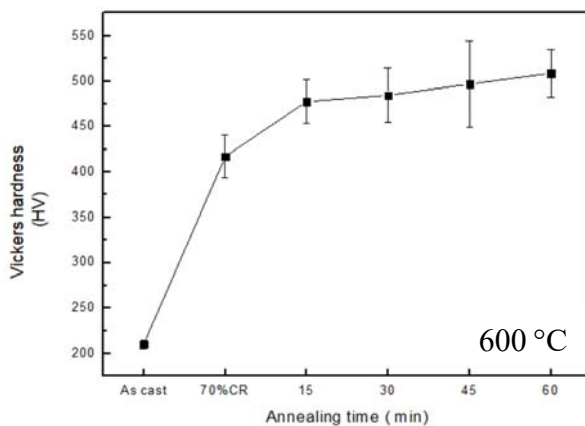


Figure 1

Figure 1. Vickers hardness as a function of annealing time for a constant temperature of 600 °C, homogenization and 70% cold rolling. Data points represent average values, bars indicate standard deviation.

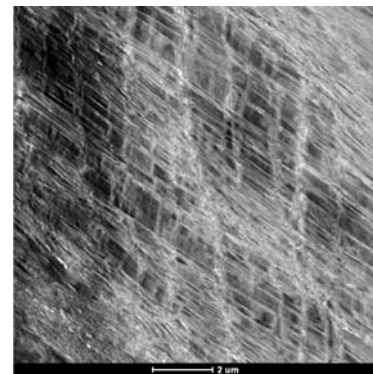


Figure 2

Figure 2. STEM-HAADF image. Deformation structures following rolling and annealing at 600 °C/1 h shows multiple deformation twins and high density dislocations.

A Novel Denoising Technique by Using Machine Learning Based Approach

Ren-Fong Cai (蔡任豐)^{1,2,*}, Mu-Tung Chang (張睦東)¹, Shen-Chuan Lo (羅聖全)¹,
Chien-Chun Chen (陳健群)^{2,3,4}

¹ Material and Chemical Research Laboratories, Industrial Technology Research Institute, Hsinchu, Taiwan

² Department of Engineering and System Science, National Tsing Hua University, Hsinchu, Taiwan.

³ Instrument Technology Research Center, National Applied Research Laboratories, Hsinchu, Taiwan.

⁴ National Synchrotron Radiation Research Center, Hsinchu, Taiwan.

* renfong@itri.org.tw

With the coming of the third age of artificial intelligence, machine learning has been successfully implemented in many fields, which changed the paradigms to feed tons of data with the answer (or label) to find the pattern that matched [1-2]. However, a limited studies addressed on the electron microscopy applications. In this study, we develop a novel denoising algorithm, kMLLS clustering algorithm [3]. As shown in figure 1, the noise of the spectra had been improved via our proposed approach. To conclude, the kMLLS clustering may provide an unsupervised route to avoid human bias and open the opportunities for automatic data processing.

References

1. P. M. Voyles, Current Opinion in Solid State and Materials Science 21 141 (2017).
2. S. Raschka and V. Mirjalili, Python Machine Learning: Machine Learning and Deep Learning with Python, scikit-learn, and TensorFlow 2nd ED, Packt, Birmingham (2017).
3. R. F. Cai, M. T. Chang, S. C. Lo and C. C. Chen, the paper is preparing to submit.

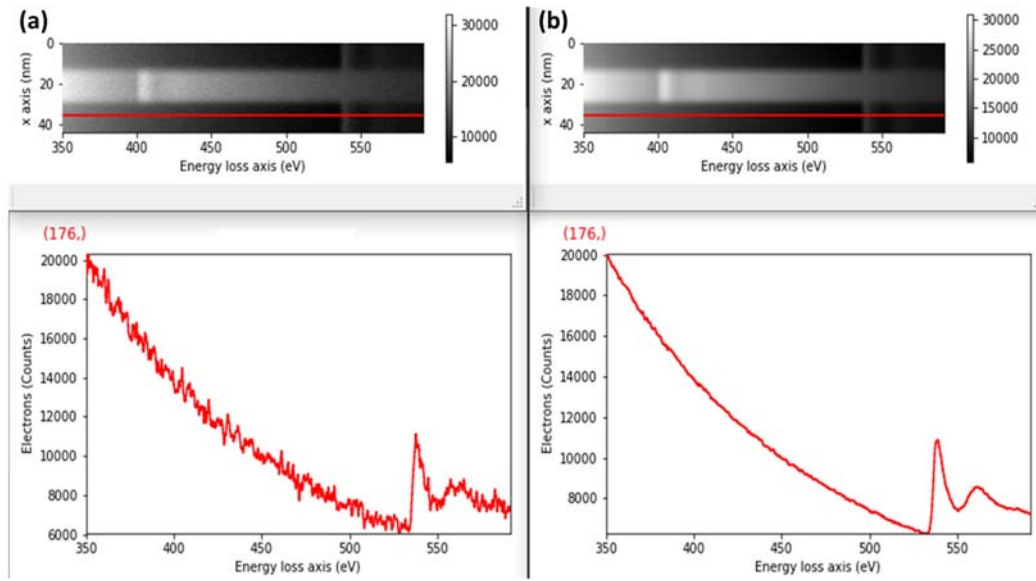


Figure 1. The comparison of the (a) experimental data and (b) kMLLS clustering denoising spectrum image and corresponding spectrum marked in it.

The Application of K-means Clustering to EELS Mapping

Ren-Fong Cai (蔡任豐),* Mu-Tung Chang (張睦東), and Shen-Chuan Lo (羅聖全)

Material and Chemical Research Laboratories, Industrial Technology Research Institute,
Hsinchu, Taiwan

*renfong@itri.org.tw

K-means clustering has been developed over half century and applied in many fields, such as image processing and feature identification, due to its elegant concept [1-3]. Due to the extended edge nature of electron energy loss spectroscopy (EELS) spectrum, multiple linear least square (MLLS) fitting was implemented to solve the overlapping issue [4]. However, the MLLS algorithm has to assign the reference spectra manually and may lead to a biased result. In this study, we introduced the k-means clustering, which extract the endmembers unsupervisedly, to an artificial EELS spectrum image. The result shows the k-mean clustering have the capability to separate the overlapping signals and give the precise distribution, and it may have a potential application in separating the different bonding state signals of the EELS spectrum image.

References

1. S. Raschka and V. Mirjalili, Python Machine Learning: Machine Learning and Deep Learning with Python, scikit-learn, and TensorFlow 2nd ED, Packt, Birmingham (2017).
2. A. Belianinov et al., Nat. Commun. 6 7801 (2015).
3. P. M. Voyles, Current Opinion in Solid State and Materials Science 21 141 (2017).
4. R.D. Leapman and C.R. Swyt, Ultramicroscopy 26 393 (1988).

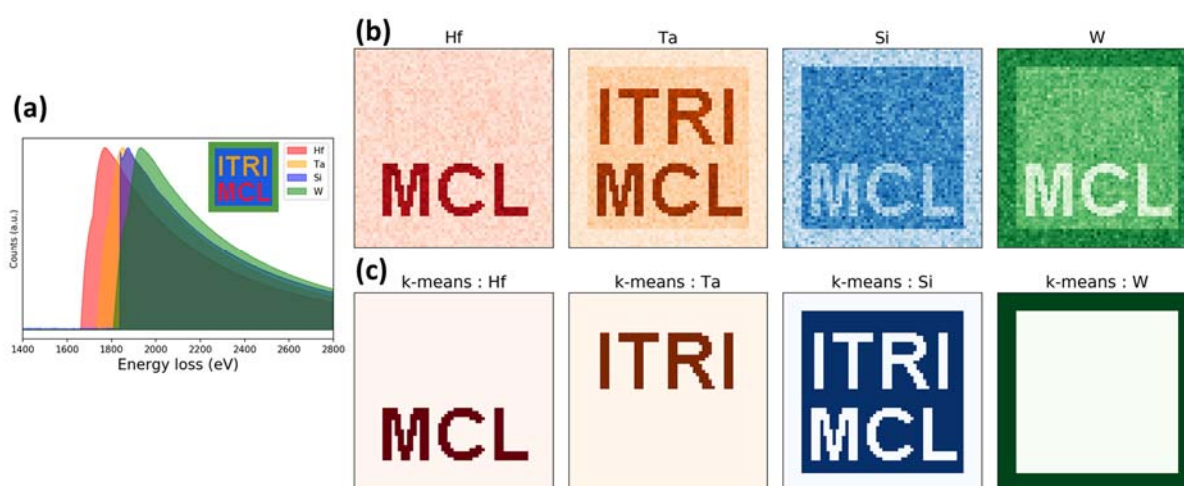


Figure 1. (a) The elemental distribution of the artificial spectrum image. (b) The distribution analysis via a ranged signal integration and (c) via k-means clustering.

Influence of tempering treatment on mechanical properties and the hydrogen embrittlement of NiCrMo steel

Shih-Chieh Kao (高士傑)¹, and Hsin-Chih Lin(林新智)¹

¹ Department of Materials Science and Engineering, National Taiwan University, Taipei, Taiwan

Martensitic steels are prone to hydrogen embrittlement, so the assessment of resistance of hydrogen embrittlement is important. In this study, hydrogen would be charged into steels by electrochemical method. By combining the results of SEM, TEM, tensile test and TDS, the relationship between microstructure and hydrogen embrittlement can be clarified. Results shows that the dominant trapping site of quench state and 200°C tempered state is dislocation; dislocation and cementite in 400°C tempered state; dislocation, cementite and M_7C_3 in 600°C tempered state. Compared with dislocation and cementite, the activation energy of M_7C_3 is higher.

Quench state shows the poorest resistance of hydrogen embrittlement with the highest hydrogen content, 0.96 ppm. The hydrogen content drops to around 0.6 ppm in 200°C tempered state and 400°C tempered state, with improvement on resistance of hydrogen embrittlement. Although 600°C tempered state has high hydrogen content, 0.95 ppm. For the lower dislocation density and stronger trapping sites, M_7C_3 , 600°C tempered state shows the best resistance of hydrogen embrittlement. 14 % elongation can be got after charging.

Precipitation Behavior in Custom 475 Maraging Stainless Steel

Cheng-Yao Huang (黃正堯),^{1*} and Hung-Wei Yen (顏鴻威)¹

¹ Department of Materials Science and Engineering, National Taiwan University, Taipei, Taiwan

*F05527001@ntu.edu.tw

In this work, the precipitation behavior of the commercial custom 475 maraging stainless steel was investigated. It was found that two kinds of precipitates present after aging, which were Ni/Al-riched β phase and $(\text{Fe,Cr})_2\text{Mo}$ Laves phase, respectively. β phase started precipitating at 480°C and retained high coherency with martensite matrix even in long aging time. β phase precipitates had sphere shape with 2-5 nm in diameter, which contributes huge precipitation hardening effect. On the other hand, Laves phase formed at 520°C and its size depended on aging time. The analysis showed that the peak aging occurs when both β and Laves precipitates meet appropriate size and distribution, and the orientation relationship between Laves phase and matrix was also determined.

References

1. Y. He, K. Yang, W. Sha, D.J. Cleland, Metall. Mater. Trans. A-Phys. Metall. Mater. Sci. 35A(9) (2004) 2747-2755.
2. J.L. Tian, W. Wang, M.B. Shahzad, W. Yan, Y.Y. Shan, Z.H. Jiang, K. Yang, Materials 10(11) (2017) 11.
3. L. Sun, T.H. Simm, T.L. Martin, S. McAdam, D.R. Galvin, K.M. Perkins, P.A.J. Bagot, M.P. Moody, S.W. Ooi, P. Hill, M.J. Rawson, H. Bhadeshia, Acta Mater. 149 (2018) 285-301.
4. S.H. Jiang, H. Wang, Y. Wu, X.J. Liu, H.H. Chen, M.J. Yao, B. Gault, D. Ponge, D. Raabe, A. Hirata, M.W. Chen, Y.D. Wang, Z.P. Lu, Nature 544(7651) (2017) 460-+.

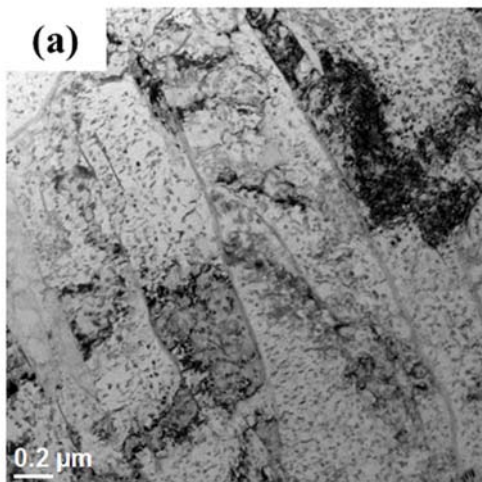


Figure 1. The TEM BF image of 520°C -4 hours aging.

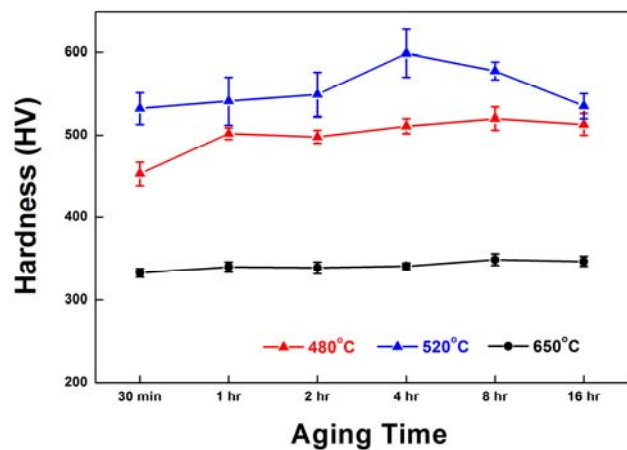


Figure 2. The overall hardness results in different aging time and temperature.

Study on the effects of Nb-Ta-Ti-V-Zr high entropy alloys composition and roughness on bone-forming cells

Wei Yu (游薇)¹, Su-Jien Lin (林世傑)², and Yi-Chia Chou (周苡嘉)^{1*}

¹ Electrophysics, National Chiao Tung University, Hsinchu, Taiwan
Hsinchu, Taiwan

² Department of Orthopaedic Surgery, Chang Gung Memorial Hospital, Linkou, Taoyuan County 33305, Taiwan

*ycchou@nctu.edu.tw

Abstract

Many attractive mechanical and physical properties were reported from various HEAs (HEAs). [1] In this poster, we investigated refractory HEA of NbTaTiVZr, which consist of the simple body-centered cubic (BCC) solid-solution phase with exceptional high yield strength and hardness that could potentially be a candidate for biocompatible metal implants. A commercial pure titanium (CP-Ti) as a conventional implant material was analyzed as a reference data. The samples were prepared using SiC sandpaper gridding to reach three conditions of surfaces including 600 grit surface, 1200 grit surface, and mirror-like surface using 0.05 μ m Al₂O₃ slurry. We then examined the behaviors of bone-forming MC3T3-E1 cells on the samples with different surface roughness. The samples with the different surface roughness may cause morphologies and cell responses differently. [2] The surface roughness of the samples was measured using alpha step. The surface wettability was characterized by the sessile drop contact angle method. The cell attachment was studied using scanning electron microscope (SEM) which shows the adhesion of cells on a rough surface was better than that on a smooth one.

References

1. L. Huang et al. (2011) " Responses of bone-forming cells on pre-immersed Zr-based bulk metallic glasses: Effects of composition and roughness" *Acta Biomaterialia* 7, 395–405.
2. H. Zhang et al. (2015) "MC3T3-E1 cell response to stainless steel 316L with different surface treatments" *Materials Science and Engineering C* 56, 22–29.

TEM Analysis of structural defects in homoepitaxial (111) diamond film on nickel-coated HPHP diamond

Kun-An Chiu (丘坤安)*, Wei-Lin Wang (王尉霖), Thi Hien Do (杜氏賢), and Li Chang (張立)

Department of Materials Science and Engineering, National Chiao Tung University, Hsinchu, Taiwan

*j73628.mse95g@nctu.edu.tw

Diamond (111) film may be required for manufacturing n-type diamond electronic devices due to its lower compensation ratio and higher incorporation efficiency of donors on this orientation [1]. However, it is more difficult to obtain high quality CVD (111) diamond than (100) one because the defect density in (111) diamond is much higher than (100) diamond under general microwave plasma CVD conditions unless growth is carried out under specific conditions [1, 2]. The TEM observation of defects in a 5 μm thick (111) homoepitaxial diamond film on Ni-coated high-pressure high-temperature (HPHT) substrate has been performed with transmission electron microscopy (TEM). For the cross-sectional TEM result as shown in Fig. 1, the continuous homoepitaxial diamond film forms after epitaxial lateral overgrowth of diamond on the Ni islands and coalescence. It is shown that the dislocation density in the diamond film is about $< 5 \times 10^8 \text{ cm}^{-2}$, which is much less than that grown without Ni. Most of the dislocations in the (111) diamond film on Ni-coated substrate are 60° and screw dislocations having Burgers vectors of $1/2\langle 110 \rangle$. The rest dislocations may be of mixed types with Burgers vectors of $1/3\langle 111 \rangle$.

References

1. A. Tallaire, J. Achard, A. Boussadi, O. Brinza, A. Gicquel, I.N. Kupriyanov, Y.N. Palyanov, G. Sakr, J. Barjon, *Diam. Relat. Mater.* **41** 34-40 (2014).
2. C. J. Widmann, M. Hetzl, S. Drieschner, C. E. Nebel, *Diam. Relat. Mater.* **72** 41-46 (2017).

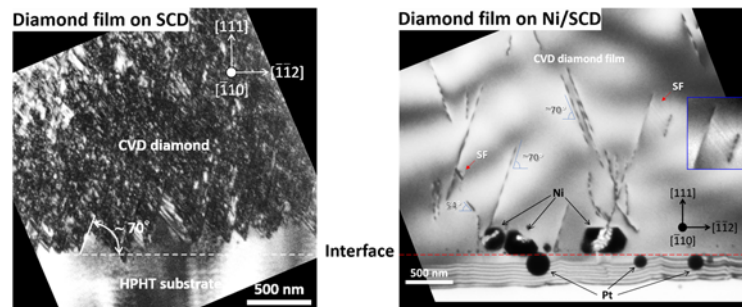


Figure 1. Bright field cross-sectional TEM image of the (111) homoepitaxial CVD diamond film on HPHT and Ni-coated substrate taken near the $[\bar{1}10]$ pole.

Study on the Effects of Different Mn Contents on Annealing and Mechanical Twinning of CoCrFeMn_xNi (X=0~1) High Entropy Alloy

Po-Han Chiu(邱柏翰),* and Jer-Ren Yang(楊哲人)

Department of Materials Science and Engineering, National Taiwan University, Taipei, Taiwan

*d07527003@ntu.edu.tw

This research focused on the difference Mn content on the annealing and mechanical twinning of CoCrFeMn_xNi high entropy alloy. After CoCrFeMn_xNi with different Mn contents were subjected to the 70% cold working and then annealed at different temperatures (700°C or 800°C) to observe the interaction between the Mn content and the annealed twin and mechanical twins. The mechanical properties were obtained by Vickers hardness test and tensile test. In addition, bullets (Semi-Armor Piercing) are used to severely deform the CoCrFeMn_xNi. The ambient temperature suppresses the effect of dynamic recovery and increases the stress, while the increase of the strain rate shortens the deformation time, the internal sliding of the material is difficult and entangled resulting in an increase in stress accumulation. The microstructure of the deformed CoCrFeMn_xNi annealed twin and mechanical twins were analyzed by TEM to investigate the role of Mn in the CoCrFeMn_xNi high entropy alloy system.

References

1. G. Laplanche, et al., Reasons for the superior mechanical properties of medium-entropy CrCoNi compared to high-entropy CrMnFeCoNi, *Acta Materialia* 128 (2017) 292-303 *Intermetallics*, 2014. 54: p. 39-48.
2. Z. Wu, et al., Recovery, recrystallization, grain growth and phase stability of a family of FCC-structured multi-component equiatomic solid solution alloys, *Intermetallics* 46 (2014) 131-140.
3. G. Laplanche, et al., Microstructure evolution and critical stress for twinning in the CrMnFeCoNi high-entropy alloy, *Acta Materialia* 118(2016) 152-163.

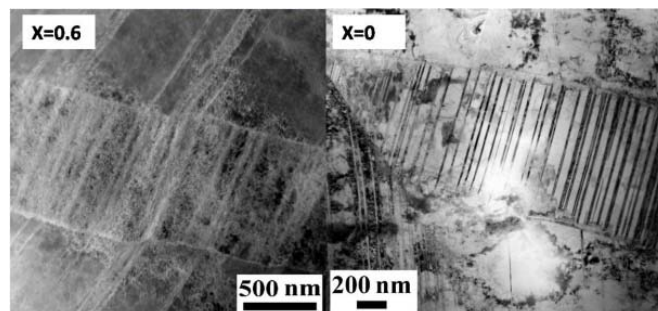


Figure 1. The severely deformed area of CoCrFeMn_xNi shot by bullet (from left to right, X=0.6, 0)

Study on Annealing Twins of Co-Cr-Fe-Mn-Ni High Entropy Alloy

Ching-Chien Chen* (陳敬謙), Po-Han Chiu (邱柏翰), and Jer-Ren Yang (楊哲人)

Department of Materials Science and Engineering, National Taiwan University, Taipei, Taiwan

*B04507008@g.ntu.edu.tw

This study focuses on the twin structure of the Co-Cr-Fe-Mn-Ni high-entropy alloy. After 70% of the cold working was applied, annealing was performed at a low temperature of 700 °C, and the behavior of recrystallization of the annealed twin crystal was observed at different annealing times. The EBSD (Electrical Backscatter Diffraction) and TEM (Transmission Electron Microscopy) analysis were used to investigate the effects of annealing on the growth of twin crystals and grain size at different annealing times. In the cold-worked 70% Cantor alloy 700 °C annealed test piece, the formation of annealed twin crystals occurs during the recrystallization and grain growth stages. Regardless of the proportion of the twin crystal boundaries, or the number of twins contained in each crystal increases with the annealing time, the reason is that there is a new twin formation inside the crystal during the grain growth stage. Moreover, since the newly grown twin crystals continue to divide the original crystal, the grain size hardly grows in the later stage of recrystallization.

References

1. Otto, F., et al., Microstructural evolution after thermomechanical processing in an equiatomic, single-phase CoCrFeMnNi high-entropy alloy with special focus on twin boundaries. *Intermetallics*, 2014. 54: p. 39-48.
2. Laplanche, G., et al., Microstructure evolution and critical stress for twinning in the CrMnFeCoNi high-entropy alloy. *Acta Materialia*, 2016. 118: p. 152-163.

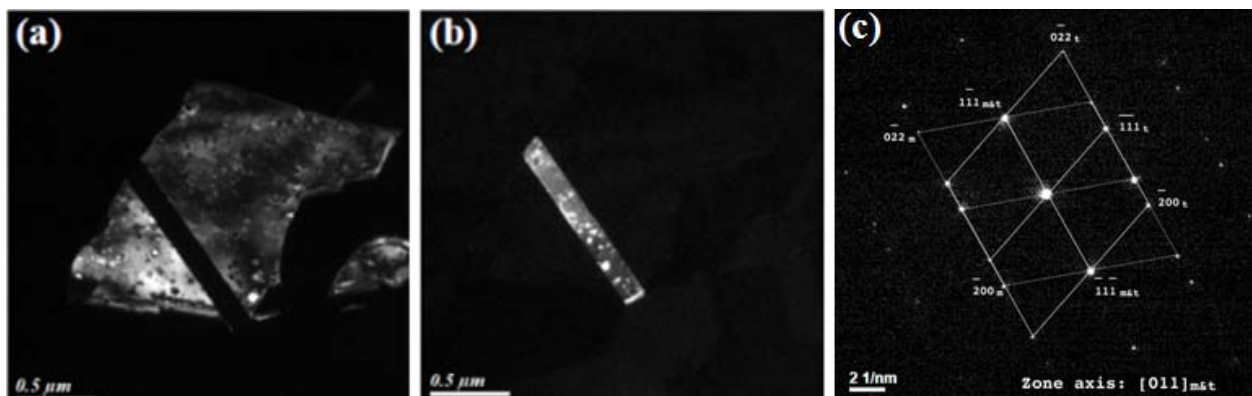


Figure 1. (a) and (b) TEM dark field images, imaged by the diffracted beams circled by the matrix and twin in (c). (c) The diffraction pattern of this region, zone axis is [011], which is a typical FCC twinning diffraction pattern.

Observing the growth and distribution of annealing twins at low annealing temperature in FeCoNiCr high entropy alloy

Yo-Shiuan Lin (林佑諠)*, and Jer-Ren Yang (楊哲人)

Department of Materials Science and Engineering, National Taiwan University, Taipei, Taiwan

* r07527032@ntu.edu.tw

A FeCoCrNi equiatomic high entropy alloy (HEA) with a single solid solution was cold rolled with a thickness reduction of ~70% at room temperature, followed by annealing treatment with relative low temperature at 650°C. In this study, the growth and distribution of annealing twins were observed at different annealing time from 10 to 60 minutes. The results show that our annealing condition (low annealing temperature and short annealing time) produces heterogeneous, partially recrystallized microstructures. The EBSD (Electron Backscatter Diffraction) and TEM (Transmission electron microscopy) analysis were used to investigate the growth and distribution of annealing twins at different annealing time.

References

1. Otto, F., Hanold, N. L., & George, E. P. (2014).
2. Laplanche, G., Kostka, A., Horst, O. M., Eggeler, G., & George, E. P. (2016).
3. Slone, C. E., Miao, J., George, E. P., & Mills, M. J. (2019).

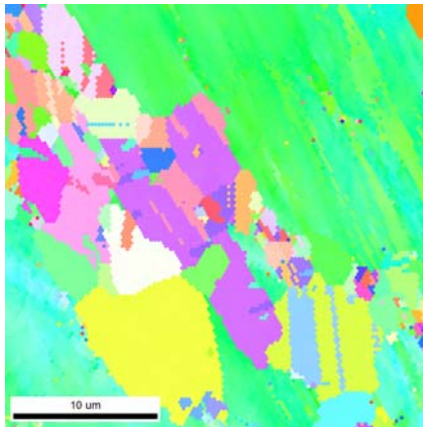


Figure 1

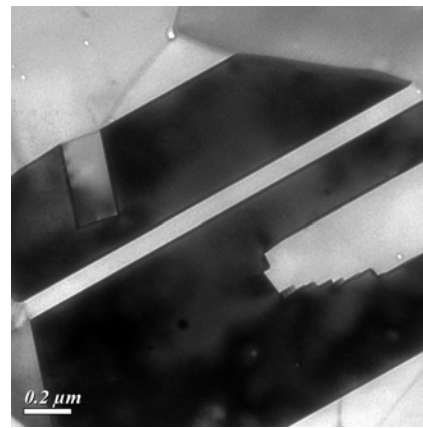


Figure 2

Figure 1. EBSD image from FeCoNiCr after rolling (70% thickness reduction) and annealing at 650 °C /1hr

Figure 2. Central dark field image. TEM from FeCoNiCr after rolling (70% thickness reduction) and annealing at 650 °C /1hr

The Effect of Two-step Heat Treatment on the Carbide-free Bainite

Ting-Mu Chung (莊庭牧)¹, Yu-Ting Tsai(蔡宇庭)²,
Yu-Wei Lai(賴昱維)^{1*}, Jer-Ren Yang(楊哲人)¹

¹ Department of Materials Science and Engineering, National Taiwan University, Taipei, Taiwan

² China Steel Cooperation, Kaohsiung, Taiwan

*r07527058@ntu.edu.tw

By alloying 1.5-2.0 wt% silicon in the steel, followed by appropriate heat treatments, carbide-free bainite can be produced. Carbide-free bainite has outstanding strength and toughness, which is well utilized in ballistic-resistant steels of defense industry, but the reaction rate is slow and it consumes much time for transformation. In this research, we are focusing on different heat treatments to accelerate the reaction rate for the transformation of carbide-free bainite. Results show that two-step heat treatment can effectively accelerate the reaction rate of carbide-free bainite, which is faster than traditional one-step heat treatment. By analyses of dilatometer data and pictures of electron microscopy, we can confirm that the final structure by two-step heat treatment consists of different size of bainite and hence results in the reduction of strength and hardness.

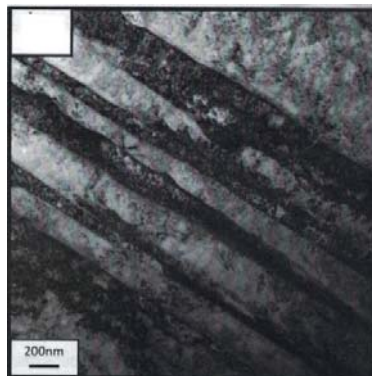


Figure 1. TEM image of bainite structure by two-step heat treatments

References

1. C. Garcia-Mateo, F.G. Caballero, ISIJ 45 (2005) 1736.
2. Caballero, F. G., Bhadeshia, H. K. D. H., Mawella, K. J. A., Jones, D. G. & Brown, P. Mater. Sci. Technol(2001). 17, 512–516.
3. A. J. Rose, F. Mohammed, A. W. F. Smith, P. A. Davies and R. D. Clarke, Mater. Sci. Technol., 2014, 30, 1094–1098.
4. C. García-Mateo, F.G. Caballero and H.K.D.H Bhadeshia, ISIJ Intl., Vol. 43, No. 8, 2003, pp. 1238-1243.

The influence of low temperature on the hydrogen embrittlement of NiCrMo steel

Li-Jen Ho(何立仁), Chih-Fu Tu(涂植夫), Hsin-Chih Lin(林新智)

Department of Materials Science and Engineering, National Taiwan University, Taipei, Taiwan

The experiment found steel in the water quenched state, is lath martensite structure, has the highest dislocation density, and observed a little self-tempered plate. After tempering at 200 °C, fine ϵ carbides began to precipitate in martensite, and the dislocation density was reduced. The hydrogen absorption after charging was the lowest, therefore it has the better resistance to hydrogen embrittlement. After tempering at 400 °C, fine ϵ carbides are transformed into cementite precipitated in temper martensite matrix. The interface between cementite and the temper martensite matrix is a reversible hydrogen trapping site, which makes the hydrogen absorption capacity is higher than 200 °C, and the hydrogen embrittlement resistance is thus lowered. When tempered at 600 °C, cementite is spheroidized. At this time, due to the elimination of internal stress during the tempering process, dislocation density is the smallest, and the best hydrogen embrittlement resistance ability is obtained in this experiment.

When doing tensile test at different temperatures, the elongation of steel decreases with decreasing temperature, but the elongation loss rate does not change significantly with temperature. It is known from experiments that both low temperature and hydrogen charging tend to cause brittle failure, but there is no obvious additive effect between them. Only in the water quenched state, the material has been destroyed before the yield strength, after tempering, the ability to resist hydrogen embrittlement has been improved.

Mechanical Property and Microstructure of Cryogenic Temperature and High-strain-rate Compressive Deformation in the FeCoNiCrMn High-entropy Alloy

Pin-Jung Chem(陳品戎)*, Jen-Ren Yang(楊哲人)

Department of Materials Science and Engineering, National Taiwan University, Taipei, Taiwan

[*r06527008@ntu.edu.tw](mailto:r06527008@ntu.edu.tw)

高熵合金作為金屬領域新興材料，近幾年來受到廣泛關注，又以 FeCoNiCrMn 作為最多人研究的系統之一。根據文獻報導，在低溫拉伸實驗中，具有低疊差能之面心立方單相結構 FeCoNiCrMn 高熵合金會生成大量機械雙晶，雙晶除了能有效阻擋差排移動亦可促使晶粒細化之效用，增加材料之加工硬化率、強度與延展性等機械性能。

本研究藉由霍普金森快速撞擊試驗機，在不同溫度(25°C、-50°C、-100°C、-150°C)和不同應變速率(4000 s⁻¹、9000 s⁻¹)對 FeCoNiCrMn 高熵合金執行壓縮變形實驗，並透過背向散射電子繞射技術與穿透式電子顯微鏡探討機械性能與顯微結構變化之影響。

實驗結果之應力應變曲線指出，隨著實驗溫度降低或是應變速率提高，材料強度皆會上升(Fig.1)，因為提升應變速率和降低溫度有著相同的效果，皆能促使機械雙晶提早形成、提高材料加工硬化率。接著透過 EBSD 和 TEM 分析材料內微結構發展，而在變形初期階段會以差排為主，隨著差排堆積、糾結使應力快速上升，達到啟動雙晶所需的臨界應力值，單一變體雙晶開始在基地中成核，且發現應力較高的條件下，其雙晶產生的數目較應力低者更多。實驗結果顯示不論在哪個應變速率或溫度，都可以觀察到機械雙晶，除此之外，結構內也觀測到兩組雙晶並存的現象，可分為基地中的 Primary twin 和 Secondary twin、退火雙晶內的機械雙晶以及機械雙晶內的機械雙晶，晚出現的機械雙晶會將原晶粒再次分割，達到晶粒細化的效果也使材料強度增強，從實驗結果可得知機械雙晶在 FeCoNiCrMn 高熵合金中是不可忽視的重要強化機制。

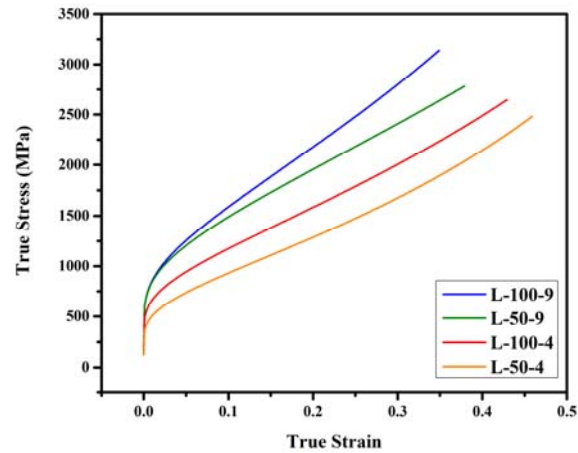


Fig.1 降低溫度或是提高應變速率皆能使材料真實應力提升(第一項 L 代表大晶粒、第二項為溫度，50 代表 -50°C 、100 代表 -100°C 、第三項為應變速率，4 代表 4000 s^{-1} 、9 代表 9000 s^{-1})

References

- [1] F. Otto, A. Dlouhý, C. Somsen, H. Bei, G. Eggeler, E.P. George, The influences of temperature and microstructure on the tensile properties of a CoCrFeMnNi high-entropy alloy, *Acta Materialia* 61(15) (2013) 5743-5755.
- [2] M.S. Christian JW, Deformation twinning, *Progress in Materials Science* 39 (1995).

Auto-tempered martensite and interpenetrating twin in lath martensite

Tzu-Ching tsao (曹梓敬),* and Jer-Ren Yang (楊哲人)

Department of Materials Science and Engineering, National Taiwan University, Taipei,
Taiwan

*tctsao@ntu.edu.tw

Fully lath martensite was obtained after quench from austenite in experimental material, not only general martensite lath but auto-tempered martensite and interpenetrating twin were able to be observed in the microstructure. Auto-tempered martensite forms from the sub-blocks which formed at high temperature. The lathes which belong to the same variant possess similar orientation relationship between each other, so when thermal energy is enough to adapt the small angle boundary, martensite will be coarsening. Because there was no high carbon region after heat treatment, the twin structure in the microstructure is interpenetrating twin instead of plate martensite. Interpenetrating twin forms from some lathes which naturally possess twin orientation relationship between each other. If the twin-relation lathes contact at the boundary of blocks, these lathes which formed at high temperature may penetrate each other to form interpenetrating twin.

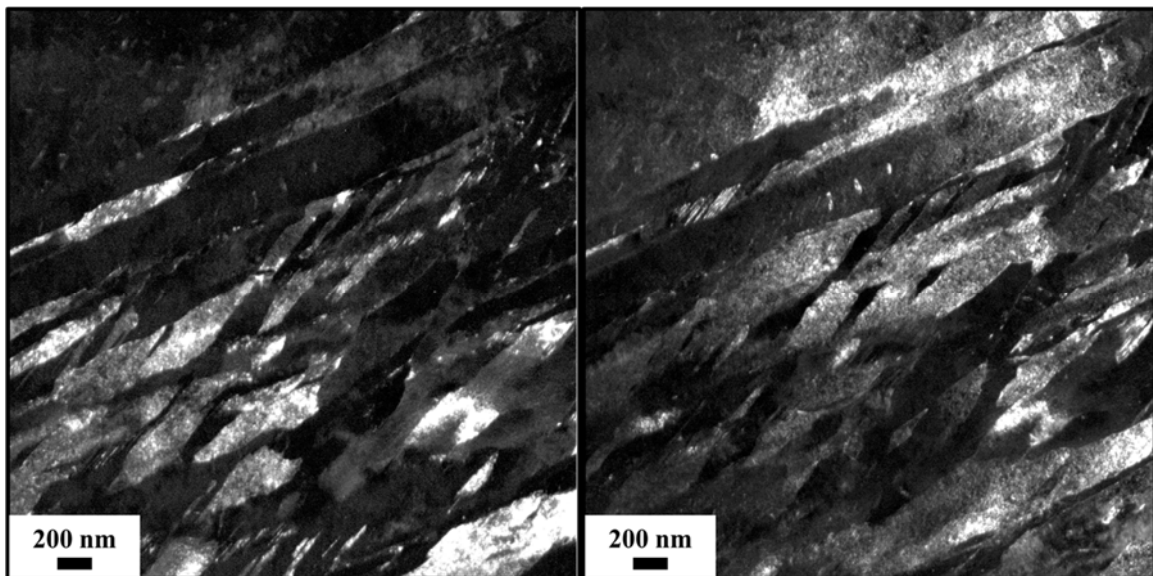


Figure 1. Dark field TEM image of interpenetrating twin.

Investigation of Strain-induced Precipitation Behavior of Niobium Micro-alloyed Steels at High Temperature

Tzu-Ching tsao (曹梓敬),* and Jer-Ren Yang (楊哲人)

Department of Materials Science and Engineering, National Taiwan University, Taipei,
Taiwan

*tctsao@ntu.edu.tw

The strain-induced precipitation behavior of niobium micro-alloyed steels at high temperature has been studied in this research. Based on the difference of niobium content, the precipitation time, precipitates size, recrystallization have been analyzed. After austenization treatment, and redissolving precipitates, materials were subjected to 25% compression deformation, and then held at the temperature we designed. According to the second compression deformation after different holding time, the degree of recrystallization of materials can be known and used to predict the time that precipitation started, and the precipitation-start time-temperature(PSTT) curve was obtained. Results reveal that different niobium content in this experiment show little effect on the start time of precipitation. The nose tip of PSTT curve is approximately in the range of 875~900°C and 2~4 second. 900°C was chosen to be the temperature for analysis because materials showed good softening resistance, slow recrystallization and early precipitation time at 900°C. Follow-up analysis shows that when niobium content is high, the size of precipitates become larger, and indication of coarsening can be observed at early stage of precipitation. Metallography also reveals that recrystallization happens more obviously when niobium content is high, indicating that more niobium may cause faster coarsening of precipitates.

Study of Self-Propagating Reaction in the Ni/amorphous-Si Reactive Multilayers

Heng Lam Kam (甘慶霖), Yuan-Wei Chang (張元蔚), Wen-Hsien Hsu (徐文賢),
Chien Chang (張阡), and Yi-Chia Chou (周苡嘉)*

Electrophysics, National Chiao Tung University, Hsinchu, Taiwan (R.O.C.)

*ycchou@nctu.edu.tw

Reactive multilayers are energetic materials composed of nanoscale interlaced exothermic reactants. By a localized ignition treatment such as a pulse laser, a portion of the multilayers intermix and release the latent heat during reaction, which further trigger the adjacent region and generate self-propagating flame. The self-propagating progress features extremely high heating (10^6 K/s) and quenching rate (10^3 K/s). [1] As a result, the temperature generally goes higher than 700 °C [2]. The propagating speed is able to reach tens of meter per second though the total amount of heat release remains small. These special characteristics enables the reactive multilayers to be applied broadly such as jointing materials and electrodes for solar cells. [3]

In this study, a series of equi-atomic Ni/Si multilayers were studied. Due to the nanoscale geometries, a scanning transmission electron microscope (STEM) was utilized to observe the surface/interfacial morphologies before and after the ignition. A transmission electron microscope (TEM) was also used to analyze the crystalline and the phase distributions. Besides, the observation of the ultimate fast self-propagating progress was achieved by a high-speed optical microscope. The results indicated that the interfacial morphologies were only affected by the pre-mixing layer while the bilayer thickness was smaller than 70 nm. Though the larger bilayer thickness indeed induced smoother interface, it elongated the diffusion distance of interlaced reactants, which significantly reduced the exothermic reaction and the consequential self-propagating speed. The self-propagating speed reached the maximum, 0.15 m/s, with the bilayer thickness of 52 nm and the total thickness of 2 μ m. The products were found majorly composed of Ni₂Si and NiSi₂ instead of the expected product, NiSi. This indicated the steady state of the faster self-propagating reaction is critical to produce the flat and uniform desired product, NiSi.

References

1. A. S. Rogachev, et al. Appl. Phys. Lett. 101: 063119 (2012)
2. I. E. Gunduz, et al. Appl. Phys. Lett. 93: 134101 (2008).
3. B. Boettge, et al. J. Micromech. Microeng. 20: 064018 (2010)

Morphology Changes of MoS₂ Nanosheets during Electrochemical Reactions in Li-ion Batteries

Chuan-Yu Wei(魏川育),* Pei-Chin Lee(李珮勤), Chin-Wei Tsao(曹晉璋), Lan-Hsuan Lee(李藍暄), and Cheng-Yen Wen(溫政彥)

Department of Materials Science and Engineering, National Taiwan University, Taipei, Taiwan 10617

*D04527001@ntu.edu.tw

Energy storage is an important issue for future technology development. For lithium ion batteries (LIBs), graphite is the most popular anode material, but the theoretical capacity is only 372 mAh/g, not high enough for future electronics. It has been demonstrated that LIBs with MoS₂ as the anode material exhibit high efficiency and high capacity. However, the cyclic stability of MoS₂, which is one of the most crucial challenges for practice applications, needs to be further investigated. In this work, we prepared MoS₂ thin films by chemical vapor deposition for the anode material in LIBs. After cyclic voltammetry measurements, TEM, SEM, and Auger electron spectroscopy are carried out to observe the morphology changes and composition of the MoS₂ anode at different charge states. The TEM and SEM results show that the MoS₂ anode has significant morphology changes, as evidenced from the formation of small islands on the anode surface after the first cycle. Besides, the AES results indicate that MoS₂ is transformed into Li₂S and Mo after several cycles. Based on these observations, we derive the mechanism of the charge/discharge processes of MoS₂ in the LIB. The findings would help us to improve the cycle stability of MoS₂ based secondary battery systems.

References

1. Zhiyuan Zeng *et al.*, In Situ Study of Lithiation and Delithiation of MoS₂ Nanosheets Using Electrochemical Liquid Cell Transmission Electron Microscopy, *Nano Letter*, 2015, 15, 5214-5220.
2. Tyler Stephenson *et al.*, Lithium ion battery applications of molybdenum disulfide (MoS₂) nanocomposites, *Energy & Environmental Science*, 2014, 7, 209-231.

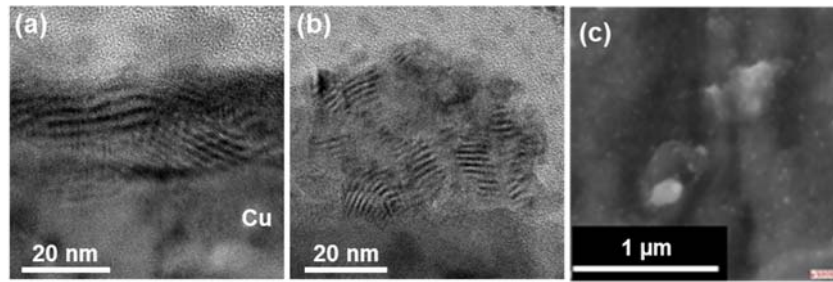


Figure 1. (a-b) Cross-sectional TEM and (c) plan-view SEM images of MoS₂ anode after the electrochemical voltammetry tests.

Chemical deviation of thermodynamic equilibrium under dynamic strain-induced austenite reversion in Mn-rich steel

Guan-Ju Cheng(程冠儒)^a, Lola Lilensten^b, Ching-Yuan Huang^c, Dierk Rabbe, Baptiste Gault^{b,*}, and Hung-Wei Yen (顏鴻威)^{a*}

^a Department of Materials Science and Engineering, National Taiwan University, Taipei, Taiwan

^b Department of Microstructure Physics and Alloy Design, Max-Planck-Institut für Eisenforschung GmbH, Düsseldorf, Germany

^c Iron and Steel R&D Department, China Steel Corporation, Chung Kang Road, Kaohsiung, Republic of China

Corresponding Author: Hung-Wei Yen, PhD homeryen@ntu.edu.tw; Baptiste Gault b.gault@mpie.de

Dynamic reversed austenite transformation was observed in a Mn-rich steel during warm tensile test between Ae_1 and Ae_3 temperature. The in-depth investigation into atomic scale of solute behavior during phase transformation-deformation coupled condition was revealed by atom probe tomography (APT) in this study. Layer-like Mn depletion zone in austenite next to the mobile phase boundary was found owing to the deviation of thermodynamic equilibrium. The present work proposed that solute partitioning value of ferrite-to-austenite transformation was lowered due to warm deformation and it was accounted for the acceleration of austenite reversion. The overall outcomes will assist the technology of warm forming of medium-manganese and lightweight steels.

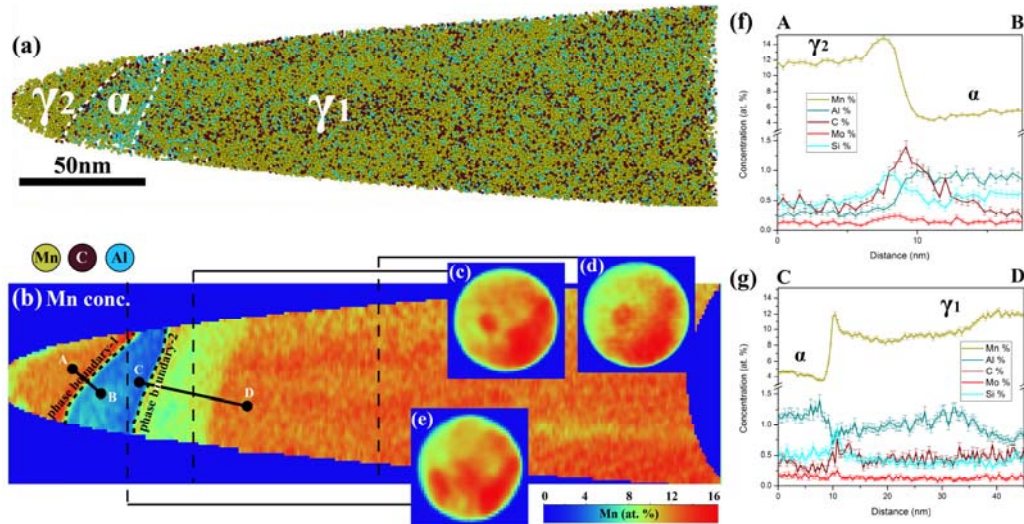


Figure 1 The APT results of the steel deformed at 10^{-3} s^{-1} for 8 min at $650 \text{ }^\circ\text{C}$ after 10 min pre-annealing: (a) The atom map of Mn, Al and C (b) The two-dimensional map of Mn concentration density and the cross-sectional ion density images within (c)(d)austenite and (e)ferrite. (f) and (g) showed the chemical composition profile across the phase boundary-1 and phase boundary-2, respectively.

Observation of SiGe Nanodots Produced by Thermal Oxidation of SiGe Thin Film

Yu-Tao Sun(孫宇韜),* and Cheng-Yen Wen(溫政彥)

Department of Materials Science and Engineering, National Taiwan University, Taipei, Taiwan

*r06527080@ntu.edu.tw

Group IV semiconductor Si/SiGe alloy heterojunction structures are potentially useful in electronics, optoelectronics, and bandgap engineering. This research focused on the growth and the properties of SiGe nanodots produced by thermal oxidation of SiGe thin films. The SiGe thin films of a low Ge content (1 at.%) is produced by ultra-high vacuum chemical vapor deposition (UHV-CVD), followed by in-situ deposition of gold nanoparticles in UHV. After the sample is oxidized at 700 °C for 6 h in air, nanodots with a higher Ge content are produced. The structures of the nanodots are examined by TEM and STEM. The results show that the nanodots are epitaxially precipitated from the eutectic AuGeSi liquid during the cooling process. The concentration, dimensional, and morphology of the SiGe nanodots can be controlled by adjusting the growth parameters.

References

1. S. A. Mala, *et al.*, Fast and intense photoluminescence in a SiGe nano-layer embedded in multilayers of Si/SiGe clusters, *Appl. Phys. Lett.* **103**, 033103 (2013).
2. H. Y. Lee, *et al.*, Producing Atomically Abrupt Axial Heterojunctions in Silicon–Germanium Nanowires by Thermal Oxidation, *Nano Lett.* **17** (12), 7494–7499 (2017).

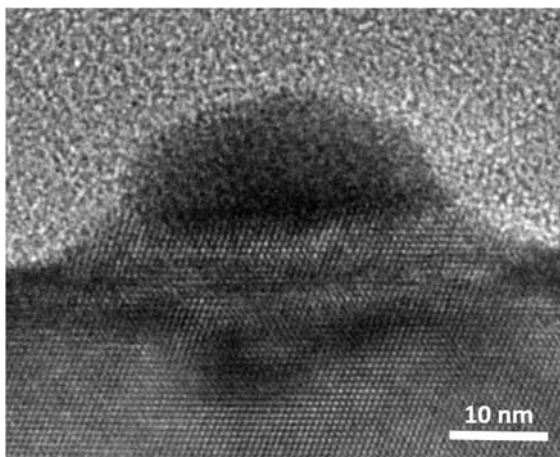


Figure 1. TEM image of SiGe nanodot.

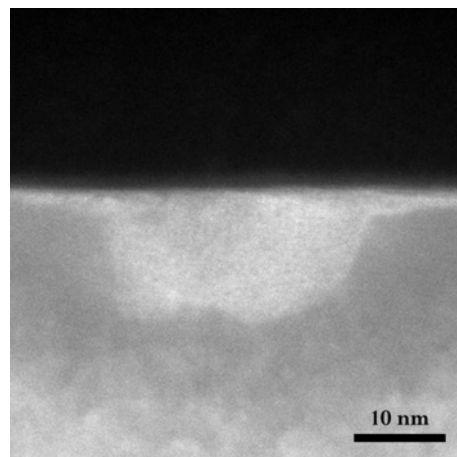


Figure 2. STEM image of SiGe nanodot after removing surface Au.

Study on Microalloyed Medium-Manganese Steels in Quenching and Austenite Reversion Process

Shan-Chun Yang (楊善淳),* and Hung-Wei Yen (顏鴻威)

Department of Materials Science and Engineering, National Taiwan University, Taipei, Taiwan

*aeee840808@gmail.com

Abstract

The micro/nanostructure and mechanical behaviors of microalloyed medium-Manganese steels processed by quenching and austenite reversion (Q&AR) were investigated. It was found that the formation of microalloyed carbide can contribute to materials' strength in two ways. During austenitization, coarser carbides enable significant grain refinement by the Zener pinning effect, leading to finer martensite laths and uniform distribution of reversed austenite in latter processes. During austenite reversion, precipitation of extremely fine carbides enables effective precipitation strengthening. Moreover, with well-controlled temperature of austenite reversion, optimized ductility can be obtained when volume fraction of retained austenite is maximized. Based on established principles, a Nb-Mo-V-adding steel was designed for optimized mechanical properties: yield strength > 700 MPa, ultimate tensile strength > 1000 MPa, uniform elongation > 14 %, total elongation > 20 %.

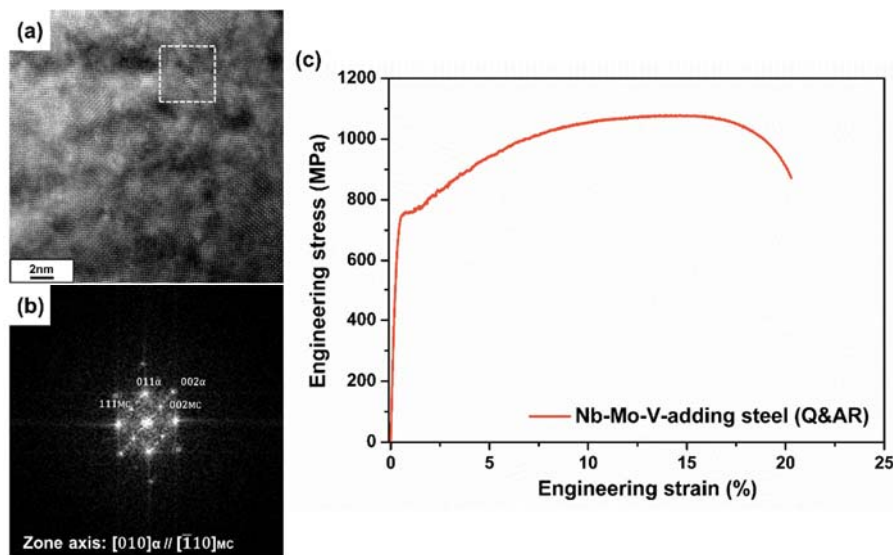


Fig.1. (a) HRTEM micrograph of microalloyed carbides and (b) the corresponding FFT diffractogram. (c) The engineering stress-strain curve of Nb-Mo-V-adding Q&AR specimen.

Reference

D. Lee, J.-K. Kim, S. Lee, K. Lee, B.C. De Cooman, Microstructures and mechanical properties of Ti and Mo micro-alloyed medium Mn steel, *Materials Science and Engineering: A* 706 (2017) 1-14.

Graphene Window for Scanning Electron Microscopy of Liquid

Yu-Yu Chen(陳昱宇),* and Cheng-Yen Wen(溫政彥)

Department of Materials Science and Engineering, National Taiwan University,
Taipei, Taiwan

*r07527037@ntu.edu.tw

Graphene is applied in a liquid cell device for scanning electron microscopy in this study. Thin Si_3N_4 membranes (<50 nm) have been adopted to seal the liquid phase for electron microscopy analysis; however, the Si_3N_4 membrane inevitably degrades image resolution. In contrast, the graphene atomic sheet has the minimum effect of electron scattering. Besides, graphene has sufficient mechanical strength for sealing the liquid in vacuum, and it is chemically inert and electrically conductive. These advantages make graphene most suitable for the window material for electron microscopy analysis of liquid phases. In this presentation, we demonstrate the fabrication of a liquid cell device in which observation can be conducted through the graphene window supported by a holey Si_3N_4 membrane. Single crystalline graphene sheets (>1 mm) were prepared using chemical vapor deposition (CVD) for the membrane material, and the fabrication procedures include photolithography, reaction ion etching (RIE), wet etching, and transferring of graphene. We show that the image resolution in the graphene viewing area is better than that of Si_3N_4 membrane (Figure 1). Such a SEM graphene/ Si_3N_4 device also shows great potential for applications because of the large liquid reservoir and the availability of flowing liquid.

Reference

1. Barin GB, et al., Optimized graphene transfer: Influence of polymethylmethacrylate (PMMA) layer concentration and baking time on graphene final performance. Carbon N Y. 84 (2015) 82-90.
2. Textor M, and de Jonge N. Strategies for Preparing Graphene Liquid Cells for Transmission Electron Microscopy. Nano Lett. 18 (2018) 3313-3321.

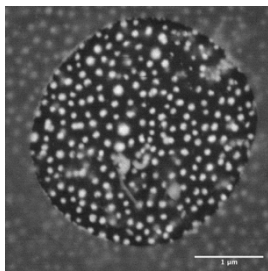


Figure 1. Back scattered electron (BSE) image of CeO_2 nanoparticles in SEM

Using Transmission Electron Microscope to Analyze the Stacking Form of Graphene Grown in Chemical Vapor Deposition

I-Ta Wang(汪奕達),* and Cheng-Yen Wen(溫政彥)

Molecule Science and Technology Program, National Taiwan University, Taipei, Taiwan

*d08551001@ntu.edu.tw

Graphene is a 2D material with a honeycomb structure of carbon atoms. Because of its unique and great mechanical and chemical properties, graphene has been applied to a lot of areas, such as biological and integrated circuits. However, with different number of layers and stacking forms, the electrical properties of graphene will be different. Therefore, determination of number and stacking form of graphene layers is very important, and Raman spectroscopy is the common and efficient instrument to determine the number of layers of graphene. We found that TEM cross-sectional images have an inconsistency result with Raman spectroscopy and SEM images of determination of number of graphene layers. In TEM cross-sectional images, we observed that there were more layers than we determined by SEM images and Raman spectroscopy. We think that the reason is because of the stacking form of graphene layers. By using the selected area diffraction method of plan-view CVD graphene, we observed that the stacking form of graphene layers is AA stacking form, which is different from the common stacking form AB stacking. This may be the reason why the inconsistency happened.

References

1. Ferrari, A.C., *et al.*, *Raman Spectrum of Graphene and Graphene Layers*. *Phys. Rev. Lett.* **97**, 18740-1-18740-5 (2006)
2. Horiuchi, S., *et al.*, *Carbon nanofilm with a new structure and property*. *Jpn. J. Appl. Phys, Part 2*. **42**, L1073-L1076 (2003)
3. Meyer, J.C., *et al.*, *On the roughness of single- and bi-layer graphene membranes*. *Solid State Commun.* **143**, 101-109 (2007)

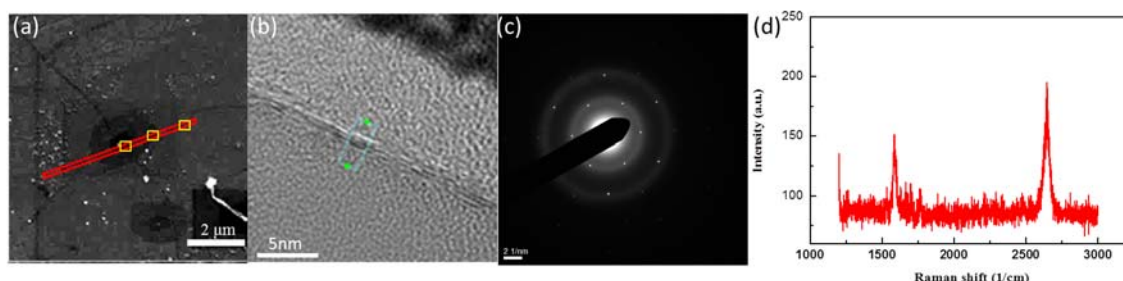


Figure 1. (a) SEM image of CVD graphene layer; (b) TEM cross-sectional image of single layer region of graphene; (c) diffraction pattern of plan-view CVD graphene; (d) Raman spectroscopy of single layer graphene.

An Investigation of Different Ageing Treatments in AA7050 Al Alloys

Yo-Ming Pua* (潘有銘), Tsai-Fu Chung(鍾采甫), and Jer-Ren Yang(楊哲人)

Department of Materials Science and Engineering, National Taiwan University, Taipei, Taiwan

*R07527A02@ntu.edu.tw

In this study, the high strength AA7075 aluminium alloys, combining with proper Cu and Mn content, are subjected to different ageing treatments such as one-step ageing treatments, two-step ageing treatments, and retrogression and re-ageing treatments, accompanying with variable degree of deformation, for molding the industrial processes (i.e., warm forming and hot stamping processes). The effect of the variable degree of deformation on the texture evolution would be analyzed by Electron Back Scatter Diffraction (EBSD). During the ageing treatment, the nano-scaled microstructural evolution of precipitates such as GP zones, η' precipitates, and η precipitates are characterized by Transmission electron microscope (TEM) and Cs-corrected high-angle-annular-dark-field scanning-transmission-electron microscopy (Cs-corrected HAADF STEM). Furthermore, the size, morphology, and volume fraction of precipitates could be quantified by Small angle X-ray scattering (SAXS). Therefore, it is a good chance to construct the microstructural evolution of precipitates related to different ageing treatments for improving mechanical properties of the high strength 7xxx series aluminium alloys in the automobile industry.

References

1. Tsai-Fu Chung, J. R. Yang, An atomic scale structural investigation of nanometer-sized η precipitates in the 7050 aluminium alloy (2019).

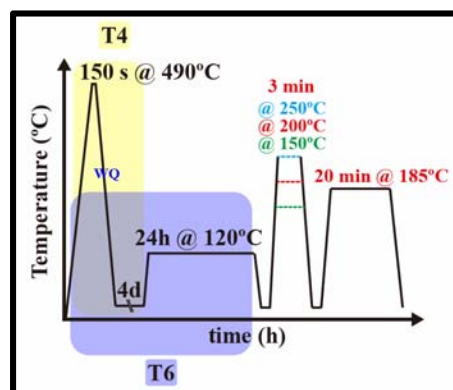


Figure 1. Simulation of heat treatment for molding the industrial processes.

Ferromagnetic Hollow Micro-spheres Composite and its SERS Application

Pei-Kai Hsu,^{1,*} Yu-Fang Huang,^{1,2} Wen-Chi Huang,¹ Shih-Yun Chen,¹ Jenn-Ming Song,³
Alexandre Gloter,⁴

¹ Department of Materials Science and Engineering, National Taiwan University of Science and Technology, Taipei, Taiwan

² Material and Chemical Research Laboratories, Industrial Technology Research Institute, Hsinchu, Taiwan

³ Department of Materials Science and Engineering, National Chung Hsing University, Taichung, Taiwan

⁴ Laboratoire de Physique des Solides, Université Paris Sud, CNRS UMR 8502, F-91405 Orsay, France

*D10804002@mail.ntust.edu.tw

In this study, iron oxide hollow spheres were prepared by spray pyrolysis method and a reduction heat treatment. The microstructure and the phase of the samples obtained in each stage were identified by electron microscopy and electron energy loss spectroscopy. The results show that the as-prepared iron oxide hollow spheres are α -Fe₂O₃. The spheres range in size from 0.5 μ m to 3 μ m with an average shell thickness of approximately 20 nm. After annealing at 350 °C for 1 hour in Ar/H₂ atmosphere, α -Fe₂O₃ was successfully phase transformed to Fe₃O₄. At 300K, the maximum saturation magnetization is 130 emu/g, which is generally higher than that of the reported form of Fe₃O₄, including bulk, nanoparticle and plate. Ag nanoparticles (NPs) were deposited on the surface of Fe₃O₄ hollow spheres. The size and spacing of Ag NPs were optimized by adjusting the synthesis parameters, which reached 5 nm and 10 nm, respectively. The SERS performance of the composite is an order of magnitude higher than the SERS performance of a solid sphere, which is attributed to the hollow structure and strong ferromagnetism H-Fe₃O₄. Finally, the composite exhibits recyclability and can be reused 8 times.

Reliability of EDS Line Profiles Extracted from Spectrum Images

Jong-Shing Bow(鮑忠興)^{1*}, Darry Chen(陳緯綺)¹, Yu-Feng Ko(葛裕逢)¹,
Chien-Nan Hsiao (蕭健男)²

¹ Integrated Service Technology, Hsinchu, Taiwan, ROC

² Taiwan Instrument Research Center, National Applied Research Laboratories, Taiwan, ROC
*js_bow@istgroup.com

EDS line profiles extracted from spectrum images are currently widely used in many TEM laboratories to analyze the composition variation through specified directions as well as to evaluate the composition of multi-thin-film materials. However, the reliability of these EDS data counted by the built-in software, especially in at%, is rarely verified in Taiwan TEM laboratories. We found the results from different STEM/EDS system were significantly difference for a multi-thin-film materials system, Si/SiO₂/SiN_x/TiON/TiN/Ta, as shown in Figure 1. This discrepancy can be minimized by modifying K-factors used in each STEM/EDS system.

References

1. G. Cliff and G. W. Lorimer, "The quantitative analysis of thin specimens", *J. Microscopy* 103, 203-207 (1975)
2. J. H. Paterson, J. N. Chapman, W. A. P. Nicholson, and J. M. Titchmarsh, "Characteristic X-ray production cross-sections for standardless elemental analysis in EDX", *J. Microscopy* 154, 1-17 (1989).
3. D. B. Williams and C. B. Carter, in *Transmission Electron Microscopy*, Chapter 35, (2009).

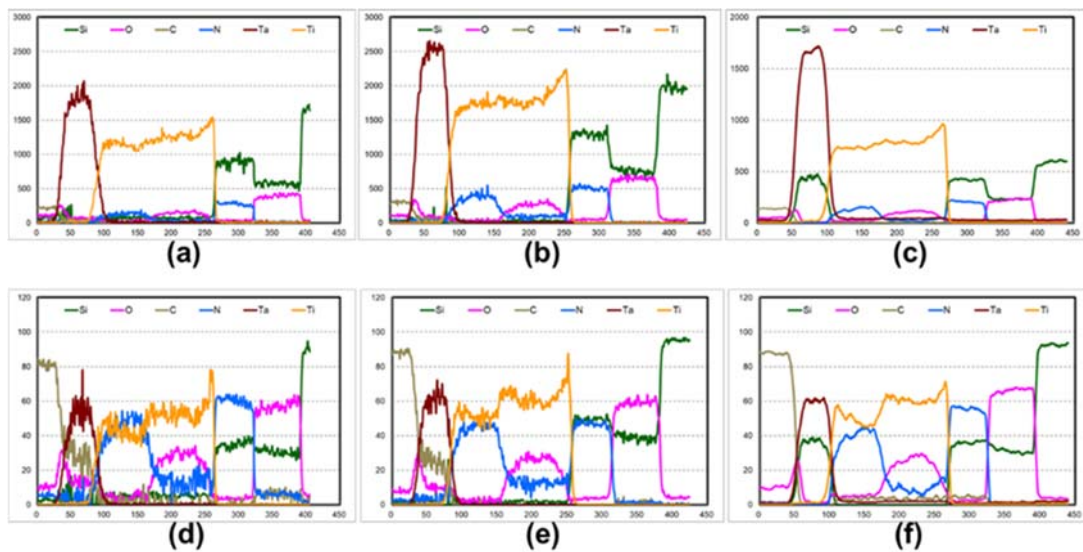


Figure 1. EDS line profiles extracted from spectrum images. (a) ~ (c) intensity line profiles from 3 STEM/EDS systems, (d) ~ (f) at% line profiles correspondingly.

Recently Progress of Lithium Ion Battery Related Environmental Stages Development in ITRI

Shih-Yi Liu (劉鈺誼), Yu-Fang Haung (黃鈺方), Chun-Wei Haung (黃浚璋), and Shen-Chuan Lo (羅聖全)*

Material and Chemical Research Laboratories, Industrial Technology Research Institute, Hsinchu, Taiwan

*AlexSCLo@itri.org.tw

Various environmental stages with the function of O₂ and H₂O isolation are essential components for investigating lithium ion battery (LIB) related topics. The environmental stages preserve the fresh bulk/surface of LIB samples and further prevent the misleading experimental result which arising from the rich-contained lithium of sample react with O₂ and H₂O among diverse analytic instruments. Material and Chemical Research Lab of ITRI has noted this eager demand from LIB research community in Taiwan and therefore developed the environmental stage for SEM observation. To expand the application function, we further design the new environmental stage to acquire the pristine x-ray photoelectron spectra with few nanometers depth below sample surface, the sample preparation procedure as depicted in fig. 1(a-c). In addition, the new function of Raman spectrum detection is integrated into previous SEM environmental stage so that complementary information of morphology, element distribution, and microstructure can be acquired from the same region which suitable for studying the lithium ion insertion/desertion at graphite anode of LIB[1], the demonstrated case as illustrated in fig 1(d-f).

References

1. C. Sole, N. E. Drewett, and L. J. Hardwick, Faraday Discuss., 172 223 (2014).

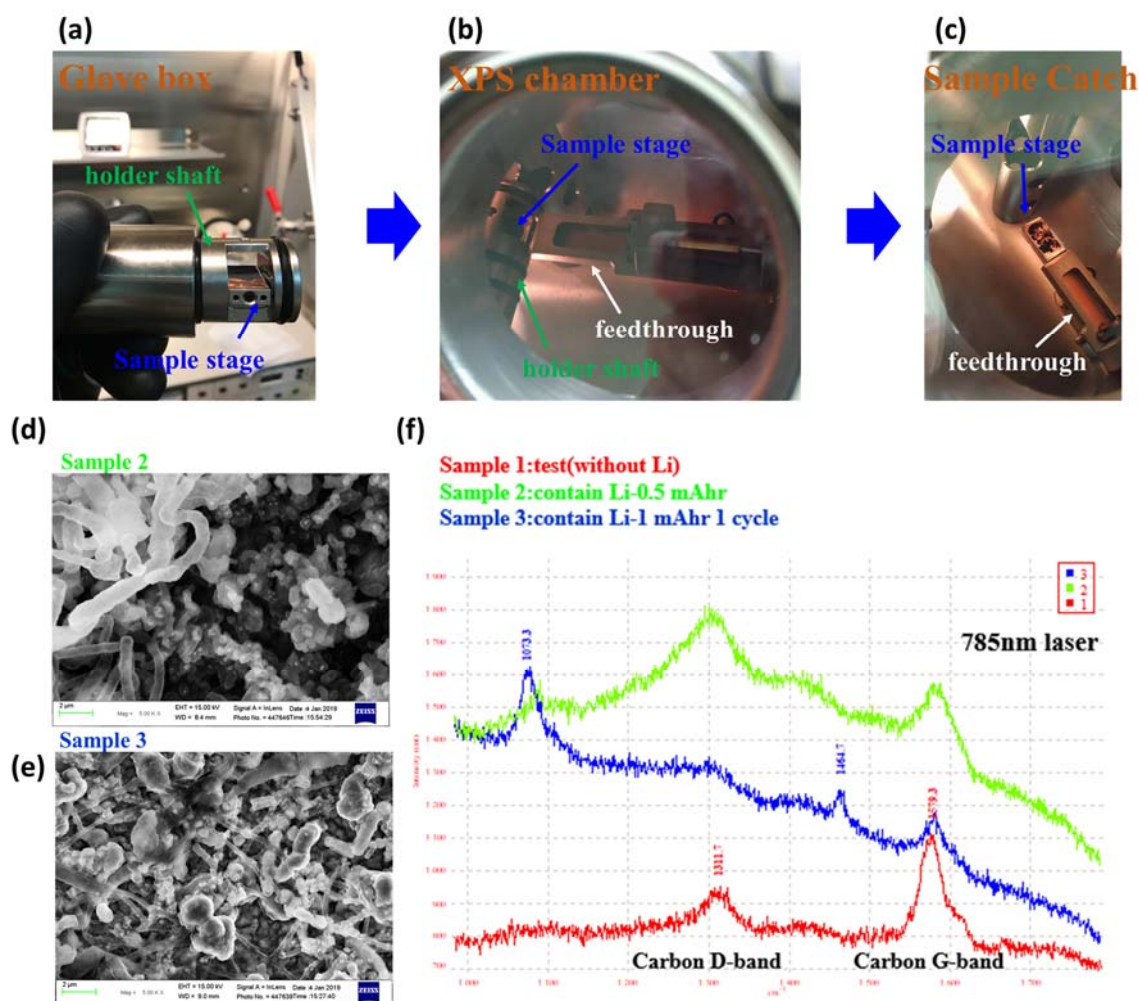


Figure 1. (a-c) Sample preparation procedure for acquiring uncontaminated XPS. (a) Sample stage puts on the holder shaft in between two o-rings for sealing. (b) The feedthrough of XPS instrument connects to the environmental protected sample stage. (c) The sample stage shifts to XPS chamber and ready to be transported. (d-f) Integrated environmental protected stage for SEM & Raman analysis. (d,e) The LIB sample morphologies of different charge/discharge condition. (f) The corresponding Raman spectra presents the different graphite anode structure.

免疫電鏡對豬流行性下痢病毒結構探討

Yu-Hsiang Chen(陳育祥)^{1,3*}, Hsiang-Ching Wang(王翔靖)², Shen-Chuan Lo (羅聖全)¹
and Hsin-Lung Chen(陳信龍)³

¹ Material and Chemical Research Laboratories, Industrial Technology Research Institute, Hsinchu, Taiwan

² Biomedical Technology and Device Research Laboratories, Industrial Technology Research Institute, Hsinchu, Taiwan.

³ Department of Chemical Engineering, National Tsing Hua University, Hsinchu, Taiwan.

*itriA00532@itri.org.tw

本研究利用免疫電鏡技術探討豬流行性下痢病毒(Porcine epidemic diarrhea virus)與受感染後之豬腸道絨毛微結構，藉此釐清豬隻受感染下痢的原因，降低未來豬隻急性感染爆發之機率。由於目前導致豬流行性下痢可能跟豬流行性下痢病毒或豬傳染性胃腸病毒有關，但由於其病毒擁有相同之病毒型態，若僅透過糞便採集往往不容易分辨。本實驗以電鏡負染前處理技術，了解 PEDV 病毒顆粒具多形性之冠狀病毒科特徵；而經其受感染後之腸檢體，可透過組織脫水切片技術，發現腸絨毛上皮微結構有空泡化和脫落的現象發生，初步推論病毒複製可能發生於腸絨毛上皮細胞質。因此，根據實驗結果，免疫電鏡技術將可協助作為病因診斷之工具之一。

References

1. 第七章 豬流行性下痢 (Porcine Epidemic Diarrhea ; PED)，取自 <https://www.baphiq.gov.tw/public/Attachment/841617155571.pdf>
2. J. A. Mascorro, B. J. J., "Processing biological tissues for ultrastructural study. In: Electron Microscopy. Methods and Protocols". Methods in Molecular Biology, Ed. John Kuo. Human Press, 2007.

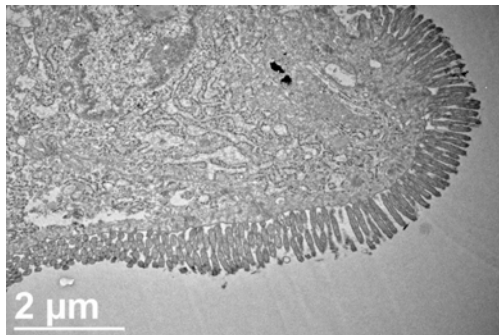


圖 1. TEM 影像之豬腸道絨毛微結構。

EPMA study on the oxidized $Tb_xDy_{1-x}Fe_{2-y}$ thin films: influence of thermal annealing on the segregation of Fe nanocluster from the oxide compositions

Chih-Hao Lee (李志浩)*, Wen-Ching Chang(張文青) and Aswin Kumar Anbalagan

Department of Engineering and System Science, National Tsing Hua University, Hsinchu, Taiwan, 30013

* chlee@mx.nthu.edu.tw

Thin films of the ternary compound $Tb_xDy_{1-x}Fe_{2-y}$ were prepared by DC magnetron sputtering from a TbDyFe alloy target with the composition same as Terfenol-D alloy $Tb_{0.32}Dy_{0.68}Fe_{1.92}$ onto 400 °C Si (001) substrates. The influence of post annealing temperature at 550 °C, 700 °C or 850 °C for 6 hours are studied systematically on a series of $Tb_xDy_{1-x}Fe_{2-y}$ samples. However, the annealing process leads to the incorporation of oxygen impurity into the thin film. To understand the effects of annealing temperature and annealing time on the microstructural and crystalline degree of oxidation of RFe₂ thin film, different characterisation techniques such as anomalous X-ray scattering and Electron Probe Micro-Analyzer (EPMA) were performed. The EPMA element mapping (Fig. 1) shows that Fe nano-clusters were surface segregated at 550 °C annealing temperature. The detailed line profiles of two nanoclusters show that these nano-Fe cluster are pure Fe cluster without Dy, Tb and O inside. This result is particularly interesting because Fe is apt to be oxidized under high temperature conditions. The possible mechanisms are found: (i) At high annealing temperatures, the Fe is segregated and form nanocluster, (ii) With the oxidation potential protection of Dy and Tb, Fe is not oxidized.

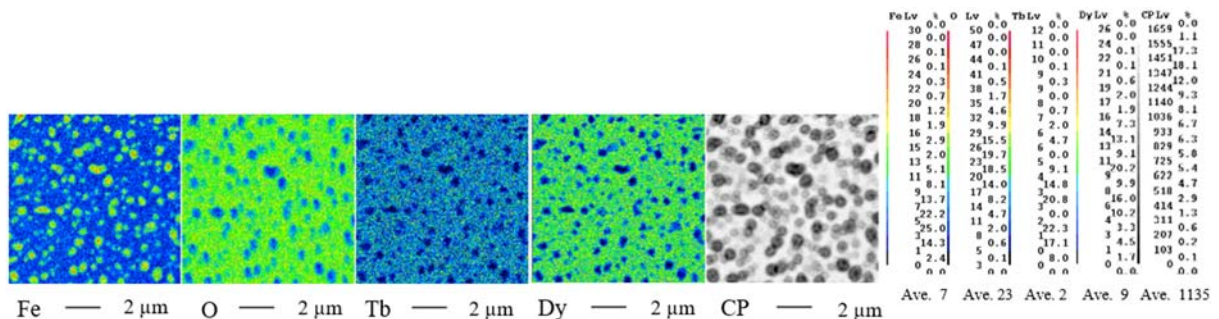


Fig. 1 Elemental maps the concentration distributions of key elements in $Tb_{0.32}Dy_{0.67}Fe_{1.92}$ thin films with the annealing temperature of 550 °C for 6 h. The CP denotes the surface morphology of the sample.

Plasmonic performance and SERS effect of meso-hollow CeO₂ spheres with Ag nanoparticles deposited

Yi-Che Chen,¹ Eric Nestor Tseng,¹ Yin-Ting Hsiao,¹ Shih-Yun Chen,^{1*}
Alexandre Gloter² and Jenn-Ming Song³

¹Department of Materials Science and Engineering, National Taiwan University of Science and Technology, Taipei, Taiwan.

²Laboratoire de Physique des Solides, Université Paris Sud, CNRS UMR 8502, F-91405 Orsay, France.

³Department of Materials Science and Engineering, National Chung Hsing University, Taichung 402, Taiwan.

*SYChen@mail.ntust.edu.tw

CeO₂ hollow spheres with Ag nanoparticles deposited (H-CeO₂@Ag) were investigated to study the role of interfaces and surface in the surface enhanced Raman spectroscopy (SERS) effect and plasmonic performance. H-CeO₂@Ag were prepared using ultrasonic spray pyrolysis followed by incipient wetness method. The diameter of CeO₂ hollow sphere ranges from 100 nm to 2 μm and the Ag nanoparticle size varies from 5 to 50 nm. Microscopy and spectroscopy were used to confirm the formation of an interface between the Ag and ceria and shows different charge rearrangements occurring at both the interface and the surface. All composites possess room temperature ferromagnetism (RTFM), which is related with ceria surface defect. A strong SERS performance was detected with a detection limit 10⁻¹⁴ M for the rhodamine 6G analyte. Scanning transmission electron microscopy (STEM) and electron energy loss spectroscopy (EELS) confirm that hot spot occurs at silver NP surfaces and Ag/CeO₂ interface.

Stoichiometric microscopy based on XANES and EELS for phase change nanomaterials

Ling Lee (李寧), Tze-Yi Yang(楊子逸), and Yu-Lun Chueh (關郁倫)*

Department of Materials Science and Engineering, National Tsing Hua University, Hsinchu, Taiwan

*ylchueh@mx.nthu.edu.tw

In this work, we demonstrated effective stoichiometric microscopy techniques to investigate the current induced phase change resistive switching random access memory (RRAM) based on copper nanowires connected by Ni electrodes. By applying a direct-current bias on copper nanowire above a threshold voltage of about 0.5 to 1 V in the atmosphere, the resistance increased significantly from several hundred ohms to several megaohms. On the contrary, a reverse polarity of external bias switches the high resistance back.

According to the shift of the absorption edges as well as the shape of above-edge oscillations extrapolated by x-ray absorption near-edge spectroscopy (XANES) and electron energy loss spectroscopy (EELS), the high resistance was attributed to the partial oxidation of copper toward Cu_2O with a degree of about 30 %. In order to furthermore combine the exact locations and the corresponding oxidation amount, scanning transmission electron microscopy (STEM) equipped EELS as well as focused synchrotron radiation nanobeam equipped XANES was utilized. In practical, the former exhibits a high resolved image with a nm-scale resolution in the cross-sectional geometry, while the latter exhibits the large-area plan-view mapping with resolution about 100 nm. Based on the results from these stoichiometric microscopy techniques shown in Figure 1, an asymmetric oxidation process between the Ni/Cu/Ni system induced by external bias was discovered, which provides a solid evidence for the design of the memristor array.

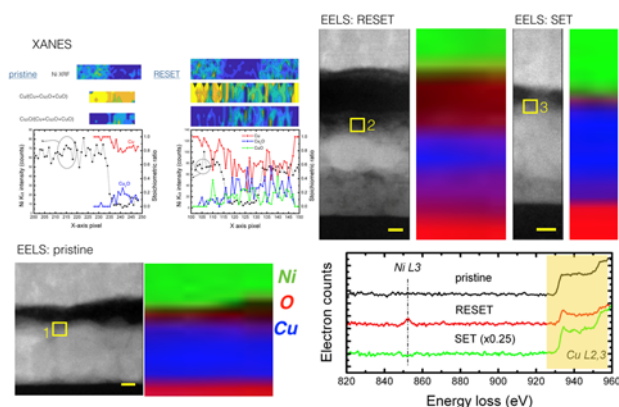


Figure 1. The XANES and EELS mapping of phase changed Ni/Cu/Ni memristor

Epochal high-performance aluminium-ion batteries based on three-dimensional molybdenum diselenide helical nanorod arrays

Tzu-Yi Yang, Shu-Chi Wu and Yu-Lun Chueh*

Department of Materials Science and Engineering, National Tsing-Hua University, Hsinchu, Taiwan, Republic of China

*E-mail: ylchueh@mx.nthu.edu.tw

The rechargeable aluminium-ion battery is a promising candidate for next-generation high-performance batteries, but its cathode materials require more development to improve their capacity and cycling life. Demonstrated herein is the growth of MoSe₂ three-dimensional helical nanorod arrays (HNRA) on a polyimides (PI) substrate by the deposition of Mo helical nanorod arrays followed by a low-temperature plasma-assisted selenization process to form novel cathodes for AIBs. The binder-free, 3D MoSe₂-based AIB shows a high specific capacity of 753 mAh/g at a current density of 0.3 A/g. Ex situ Raman, XPS and TEM results confirm the reversible alloying mechanism (Al-Se and Al-Mo) during the discharge and charge cycles. Further exploratory work on interdigital flexible AIBs and stretchable AIBs was demonstrated, exhibiting a steady output capacity under different bending and stretching states. This method provides a new and controllable strategy for selenide nanostructure-based AIBs for use in future applications of energy-storage devices in flexible and wearable electronics.

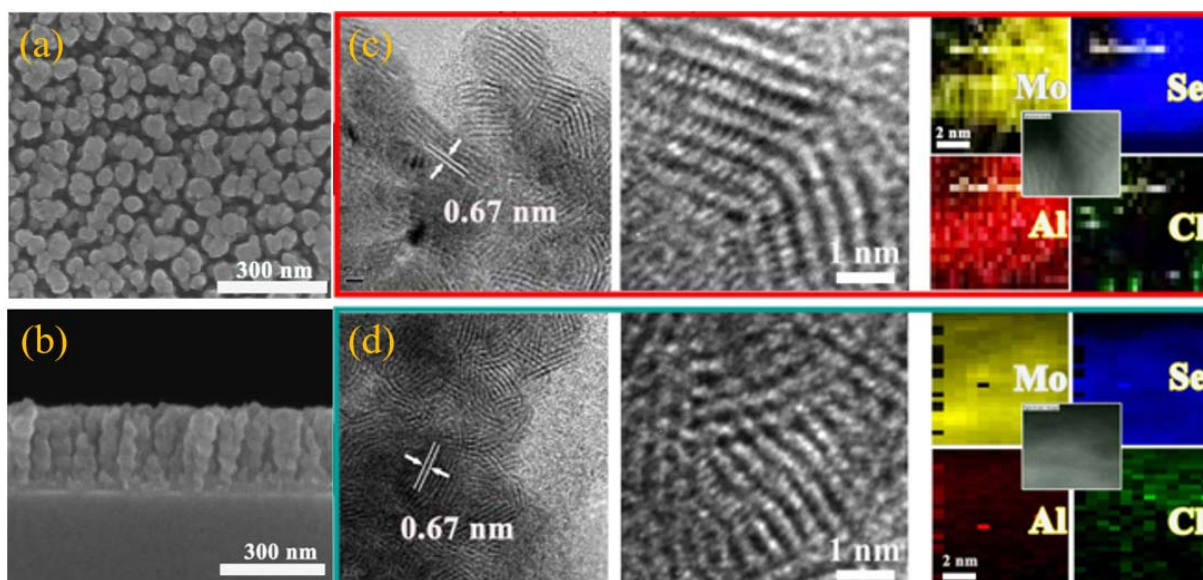


Figure 1. (a-b) SEM image of helical nanorod arrays (a) top view and (b) cross-section. (c-d) TEM and EELS mapping: (c) discharge state and (d) charge state.

Epitaxial growth of zirconium nitride grown on Si substrate by reactive magnetron sputtering

Thi-Hien Do (杜氏賢)*, Yih-Yang Tseng (曾奕洋), Kun-An Chiu (丘坤安), and Li Chang (張立)

¹ Department of Materials Science and Engineering, National Chiao Tung University, Hsinchu, Taiwan

*dohienvl@gmail.com

Zirconium nitride (ZrN) belongs to the family of transition metal nitrides and exhibits high hardness, excellent electrical conductivities, and chemical stabilities [1]. Therefore, ZrN can be considered as a potential candidate in a wide range of applications such as decorative coating, silicon CMOS technologies, and integrating plasmonics [2].

This study reports the successful growth of epitaxial ZrN thin film on Si substrate by reactive magnetron sputtering. Coating properties of deposited film such as morphology, composition, resistivity, lattice parameter were investigated as function of growth parameter. The chemical composition of the coating films was determined by x-ray photoelectron spectroscopy and Energy-dispersive X-ray spectroscopy. The thin film morphologies were analyzed by atomic force microscopy (AFM) and Scanning Electron Microscope (SEM). X-ray diffraction results and transmission electron microscopy analyses show that the epitaxial relationship between ZrN and Si is ZrN (100) // Si (100), and ZrN [011] // Si [011].

References

1. Gururaj Naik, Jongbum Kim, Nathaniel Kinsey, Alexandra Boltasseva, in [Handbook of Surface Science](#), (2014) chapter 6
2. A.B. Mei, B.M. Howe, C. Zhang, M. Sardela, J. N. Eckstein, L. Hultman, A. Rockett, I. Petrov, J. E. Greene, *J. Vac. Sci. Technol. A*, 31(2013) 061516.

Study of annealing twin on CoCrFeMnNi high-entropy alloy

Tulustia Japanesa¹, Shao-Pu, Tsai², Pin-Jung, Chen², Akhmad A. Korda¹, Jer-Ren, Yang²

¹ Department of Metallurgical Engineering, Bandung Institute of Technology, Indonesia

² Department of Materials Science and Engineering, National Taiwan University, Taiwan

CoCrFeMnNi High Entropy Alloy (HEA), which reported to have a single face-centered-cubic crystal at high-temperature, has been verified to exhibit good combination of strength and ductility which contributed by twinning formation considering its low stacking fault energy [1]. In the present work, the behavior of annealing twin of CoCrFeMnNi HEA is studied by subjecting the alloy to several temperature of heat treatment. The trend of hardness in different area of the grain was also observed. With increased of annealing temperature, increased of equiaxed grain size with change of modality of grain size distribution were observed. Annealing twin density were exhibited to have inverse correlation with grain size, due to mechanisms during grain growth [2]. Grain boundary was found to be the hardest area of the grain, and twin boundary was confirmed to be less effective than grain boundary with 4.46% deficiency of hardness.

References

[1] Yeh, J.W., Physical Metallurgy of High-Entropy Alloy, JOM, 67, (2015), No.10

[2] Jin, Y., Bernacki, et.al, Metals, 6, (2015) 5-18

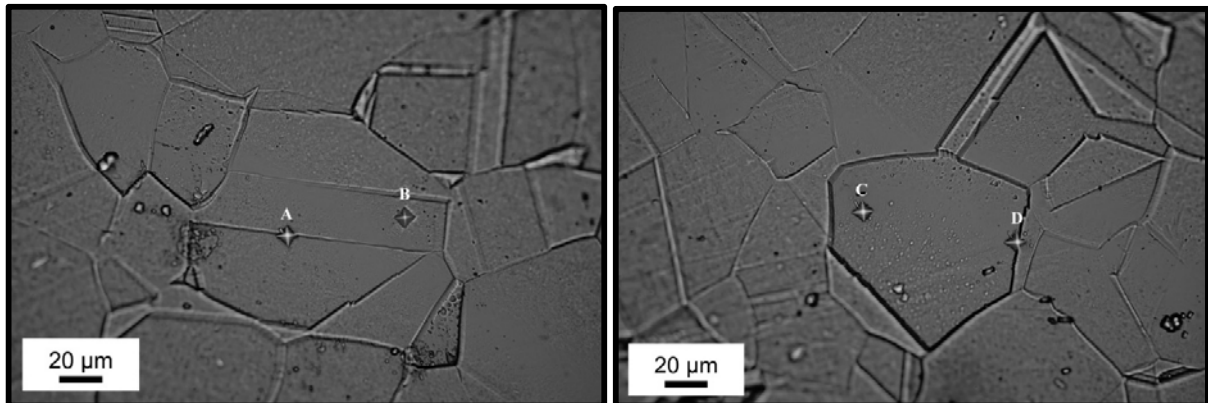
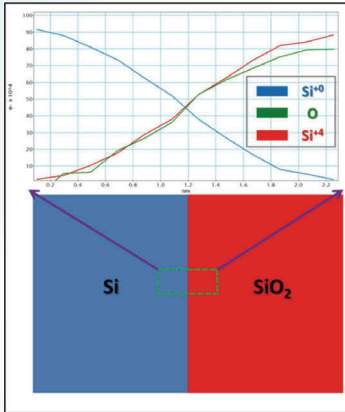


Figure 1. Optical microscopy images at different point for hardness observation in different area of the grain after annealed at 1000°C for 1 h.

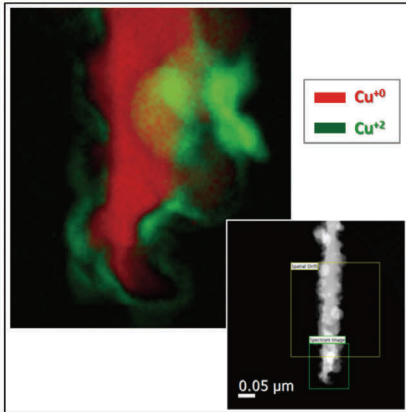
全方位奈米電鏡檢測服務提供者

電鏡高階能譜分析-原子鍵結解析技術

Case #1 - IC device

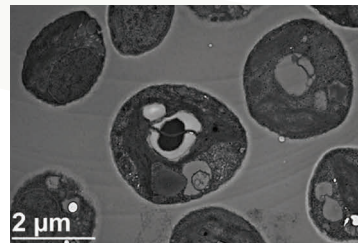


Case #2 - CuO/Cu nanowire

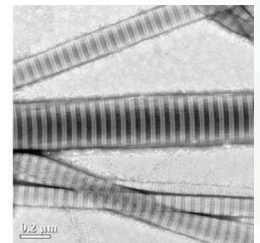


低溫電鏡技術-生物與醫藥材料之檢測

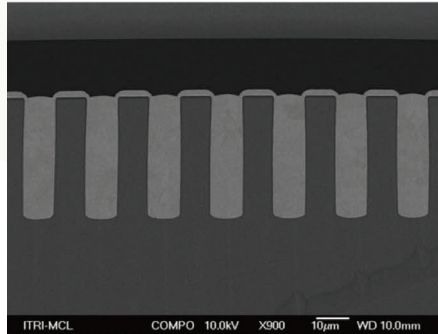
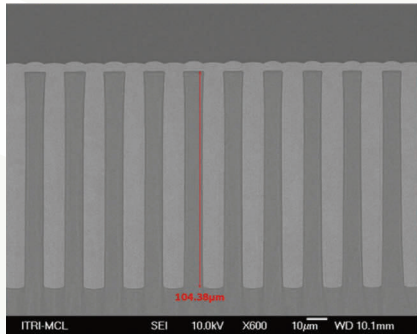
單細胞綠藻 (衣藻)



膠原蛋白

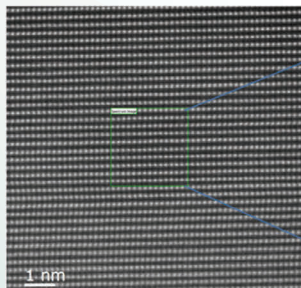


前瞻樣品製備技術 (超高平坦化樣品製備技術 CP)

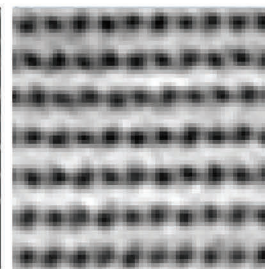
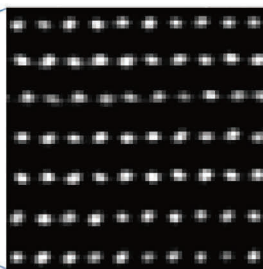


球差校正電鏡分析-次原子解析能譜影像

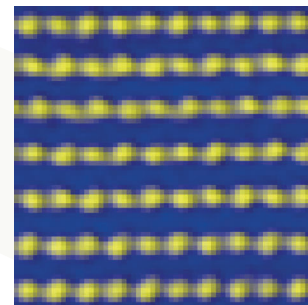
HR image (SnO₂)



Sn chemical mapping O chemical mapping



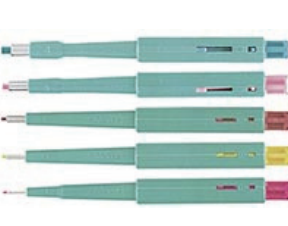
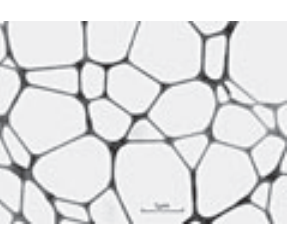
Color mixing
Sn + O chemical mapping



Sputter Coater

 <p>208HR High Resolution Sputter Coater for FE-SEM</p>	 <p>108 auto Sputter Coater</p>	 <p>108 manual Sputter Coater</p>	 <p>Targets for Sputter Coaters</p>
--	--	---	--

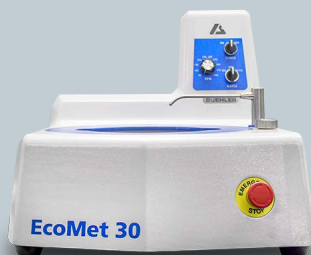
Supplies / Accessories

 <p>Adhesives Conductive SEM Nonconductive</p>	 <p>Adhesives Nonconductive Tabs/Tapes Adhesives Conductive Tabs/Tapes</p>	 <p>Coring Punches with Plungers</p>	 <p>Tweezers</p>
 <p>TEM Grids</p>	 <p>TEM Grid Storage Boxes</p>	 <p>FIB Supplies</p>	 <p>TEM Support Films</p>

電顯試片前製備儀器及耗材



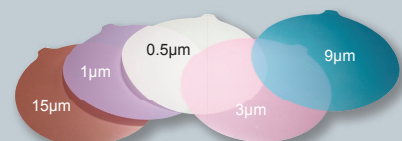
IsoMet
慢速精密切割機



EcoMet 30
手動研磨拋光機



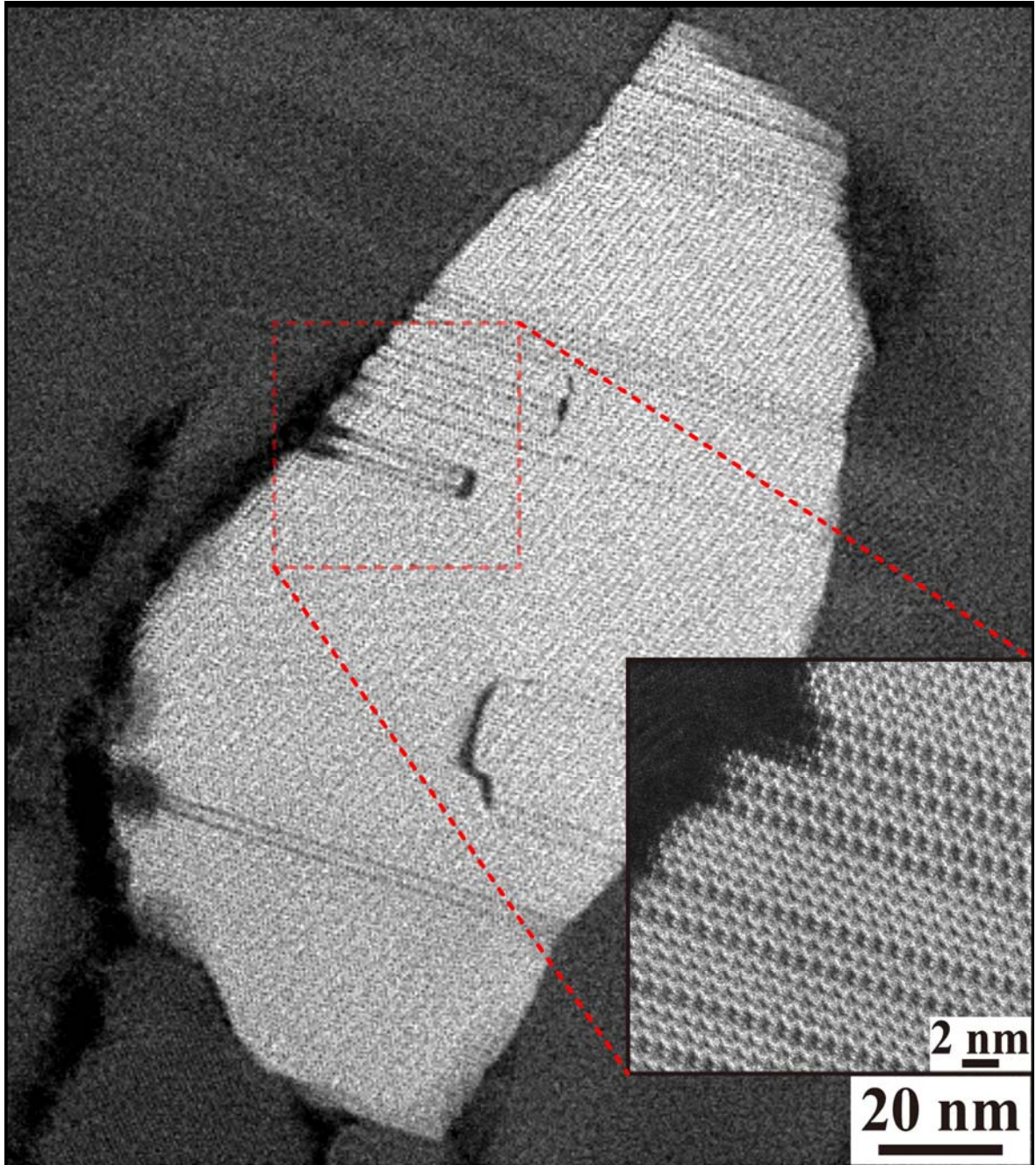
MasterMet
二氧化矽最終拋光懸浮液



鑽石拋光膜 (鑽石砂紙)

第三十九屆臺灣顯微鏡學會年會攝影比賽影像集

P-01	有你真好 台灣 鍾采甫 李威志 鮑忠興 蕭健男 楊哲人 國立台灣大學材料所	53
P-02	析出物你走了心 李威志 鍾采甫 Makoto Shiojiri 蕭健男 楊哲人 國立台灣大學材料所	54
P-03	核「心」 周晶瑩 清華大學工程與系統科學	55
P-04	熱氣球 陳穎 清華大學工程與系統科學所	56
P-05	靈光一閃 王達璋 中山大學物理學系物理所	57
P-06	Fe-Co-Ni-Cr 四元高熵合金內的退火雙晶 林佑誼 國立台灣大學材料所	58
P-07	凍湖魚群 曹梓敬 國立台灣大學材料所	59



作品名稱: 有你真好



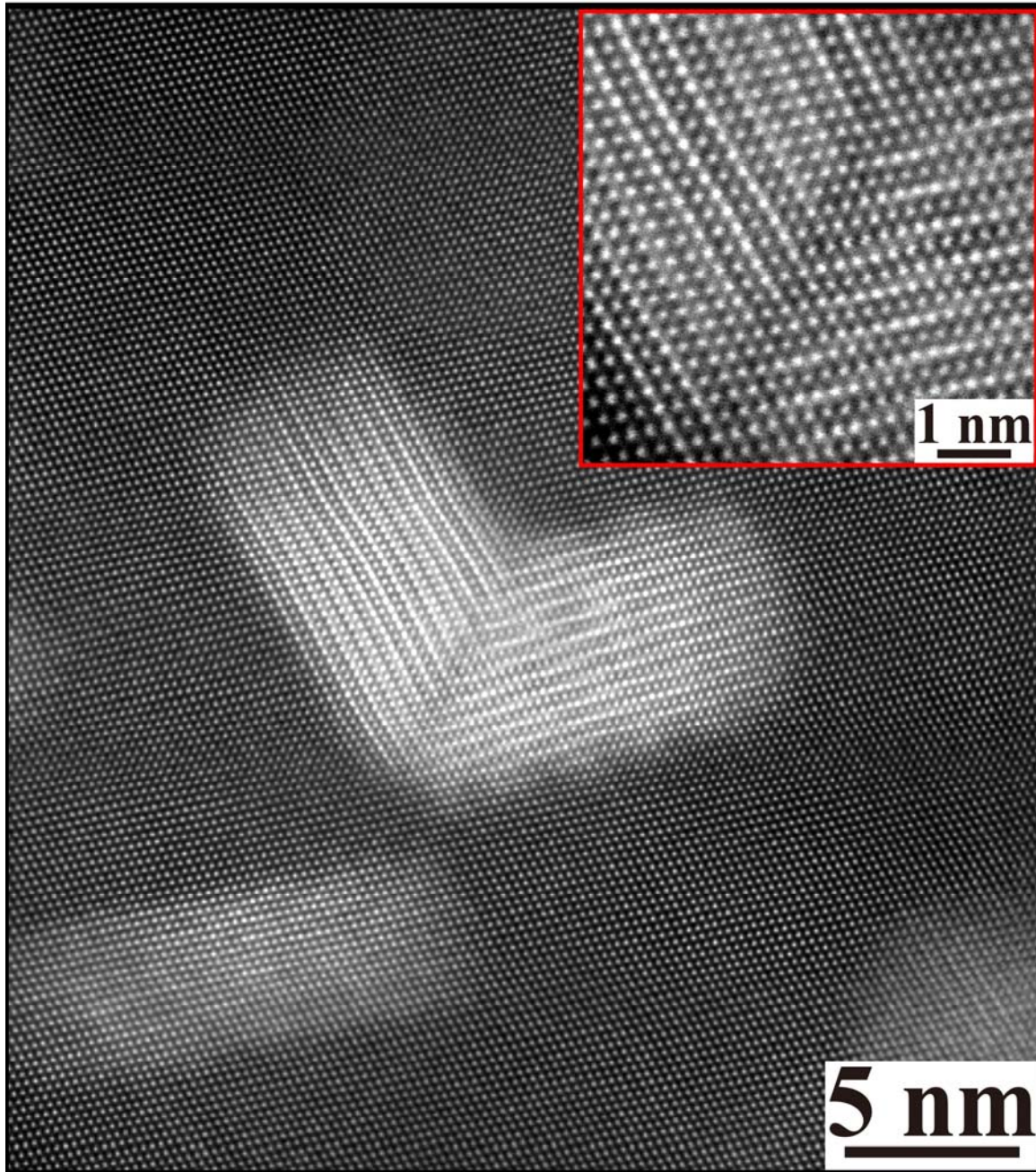
作品內容

外形似台灣的和闐玉原子級顯微影像,揭開單斜角晶系透閃石之晶體結構,交錯的原子疊差排列且原子層與原子層之間以雙晶結構進而呈現國家級古玉的神秘面紗.

作者姓名 鍾采甫,李威志, 鮑忠興,
蕭健男,楊哲人

學校單位 國立台灣大學材料所

E-Mail f03527003@ntu.edu.tw



作品名稱：析出物你走了心

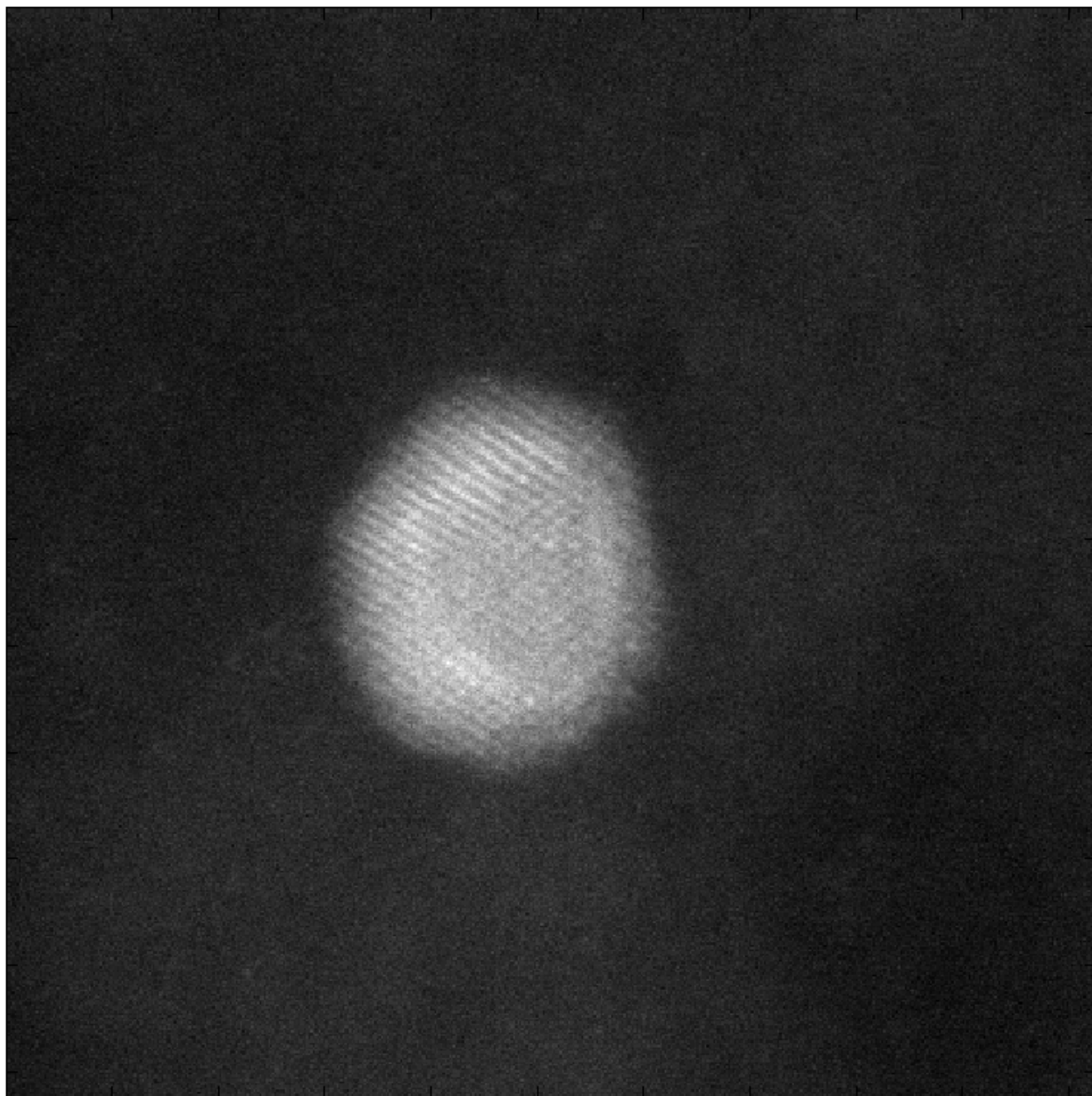
作品內容

In the AA7050 (Al-Zn-Mg-Cu), the twinning morphology of η precipitates alloy grown on the respective $(11\bar{1})_{Al}$ and $(\bar{1}1\bar{1})_{Al}$ planes, and possess a relationship with an angle of 109.5° between the $(002)_{Al}$ plane.

作者姓名：李威志,鍾采甫,Makoto Shiojiri,
蕭健男,楊哲人

學校單位：國立台灣大學材料所

E-Mail: f03527003@ntu.edu.tw



作品名稱 核「心」

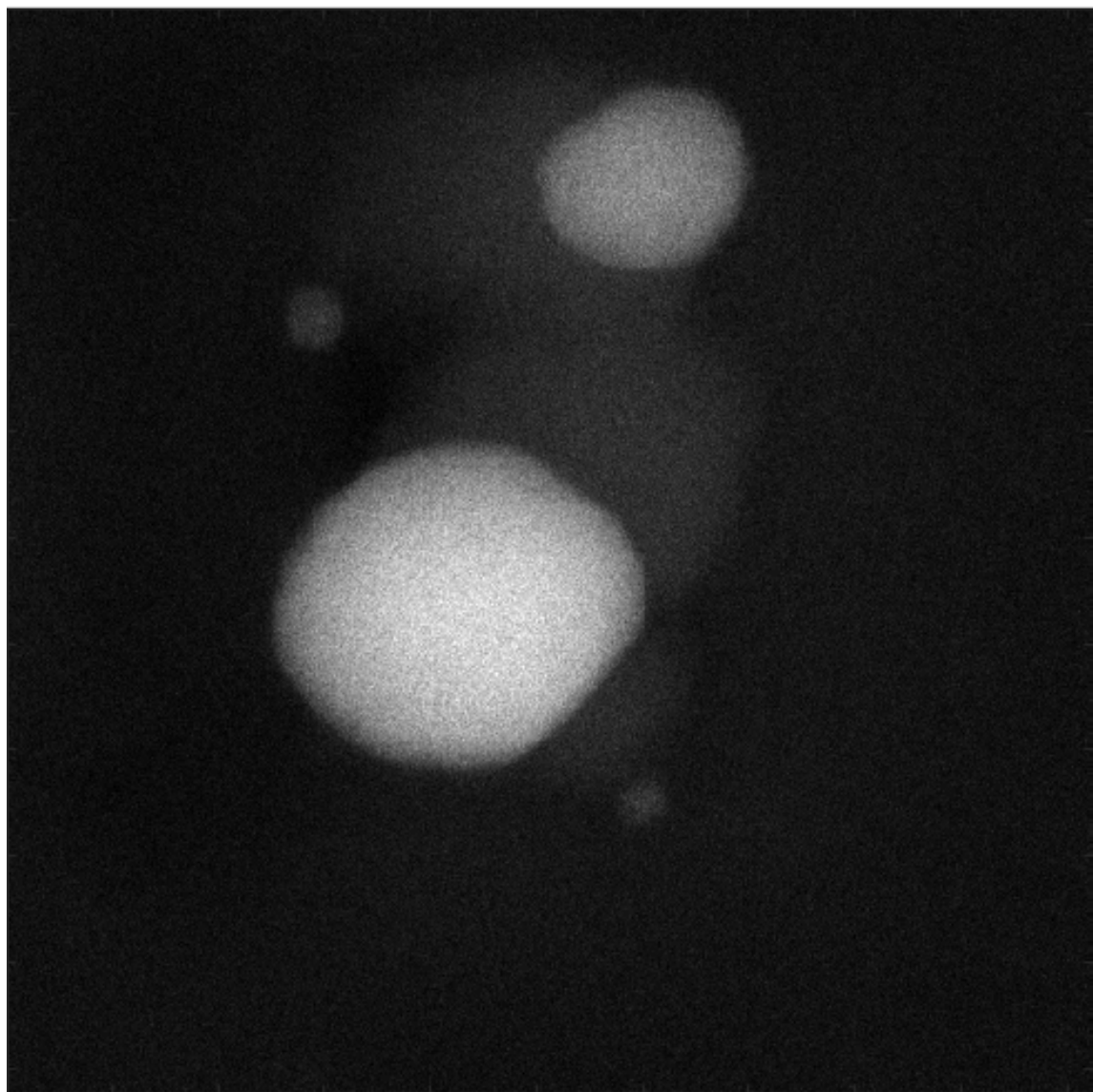
作品內容

奈米粒子 PtRuAu，在 STEM 之下，Pt(shell)包裹著 Ru(core)，其核心中映照著真心。

作者姓名 周晶瑩

學校單位 清華大學工程與系統科學

E-Mail crystal21320@gmail.com



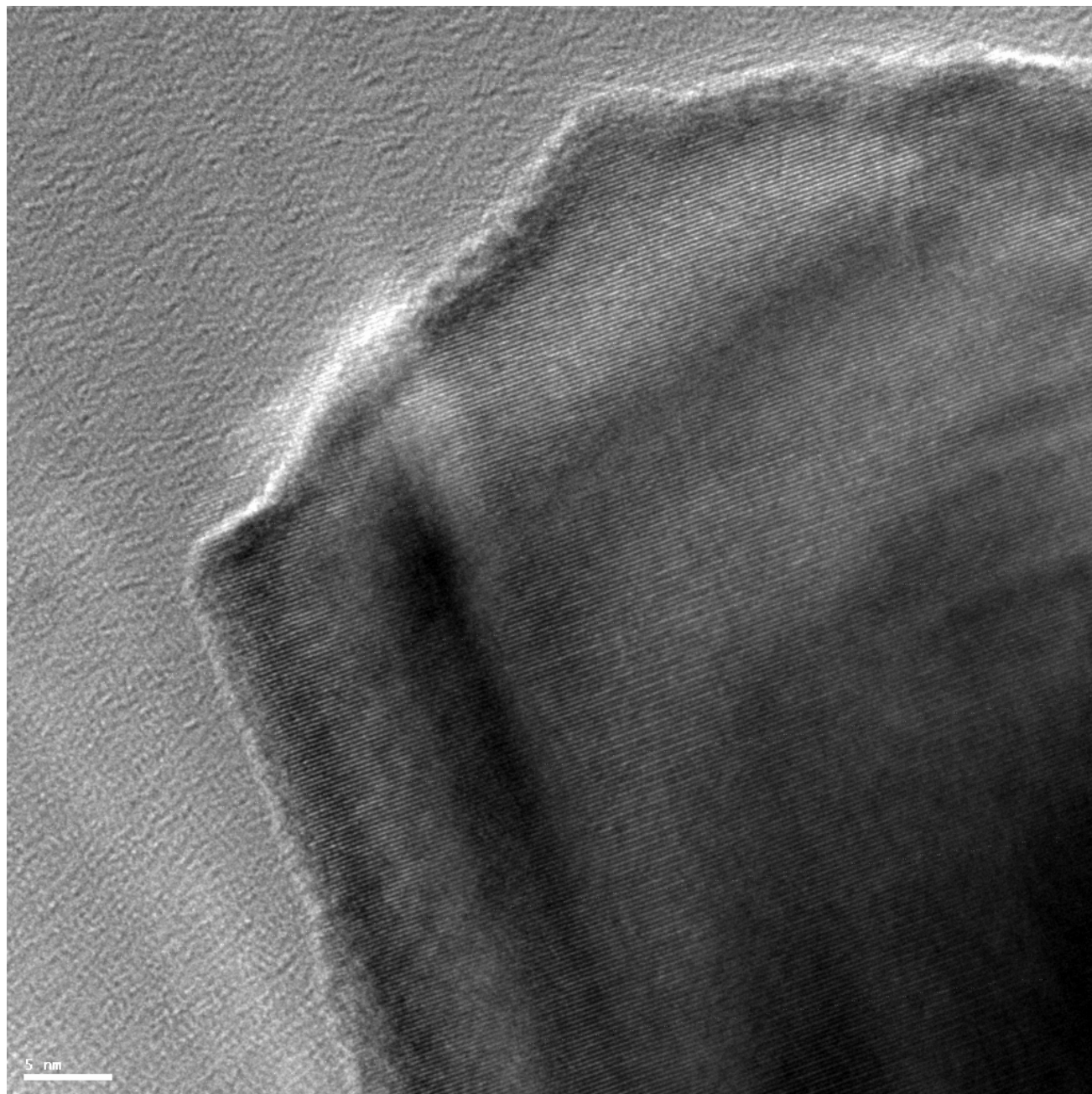
作品名稱 熱氣球

作品內容 鐵金粒子

作者姓名 陳穎

學校單位 清華大學工程與系統科學所

E-Mail in1013in@gmail.com



作品名稱: 靈光一閃

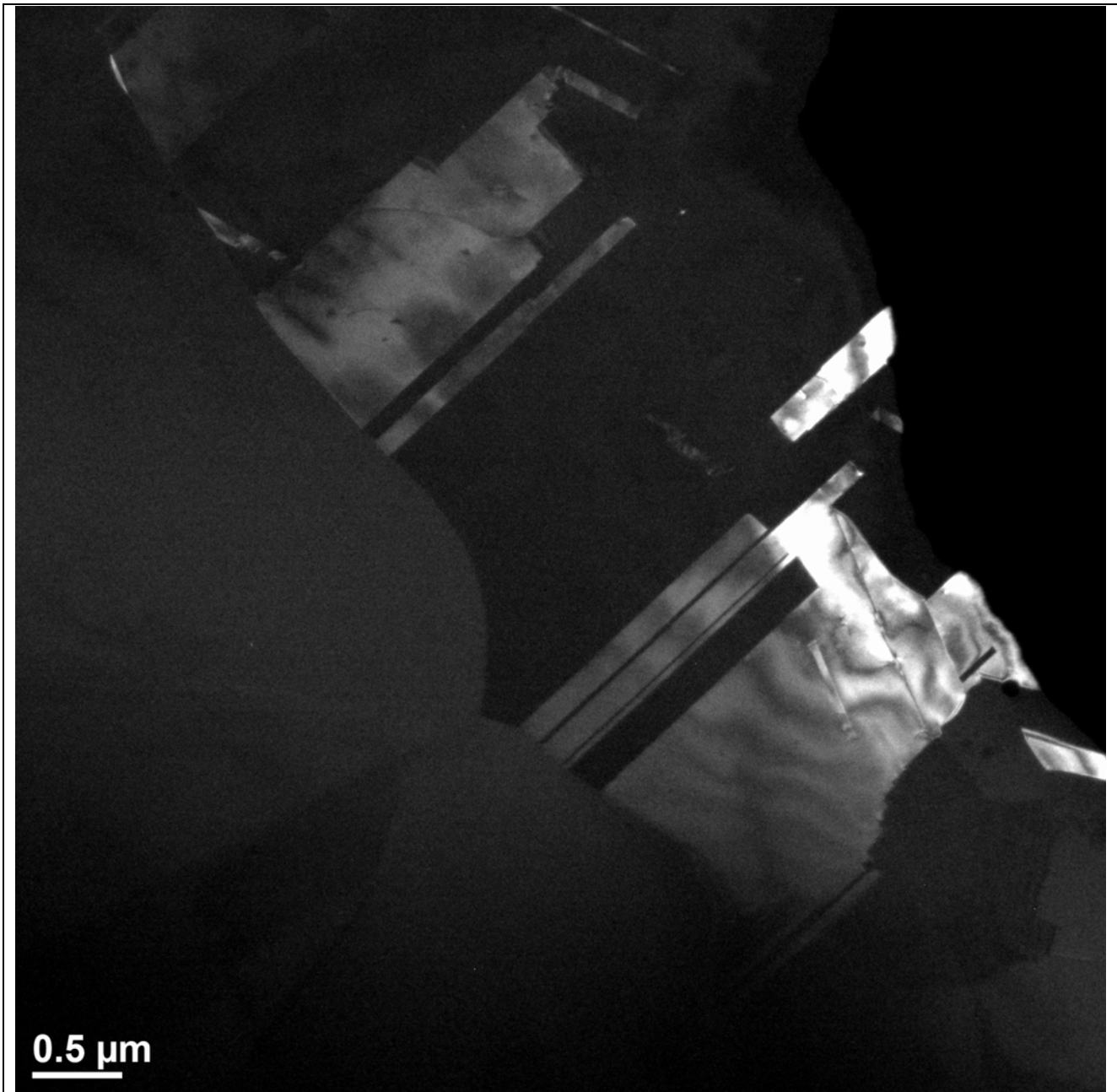
作品內容

頭頂出現一道亮光，瞬間好像明白了些什麼似的。

作者姓名: 王達璋

學校單位: 中山大學物理學系物理所

E-Mail: 520d21184@gmail.com



作品名稱 Fe-Co-Ni-Cr 四元高熵合金內的退火雙晶

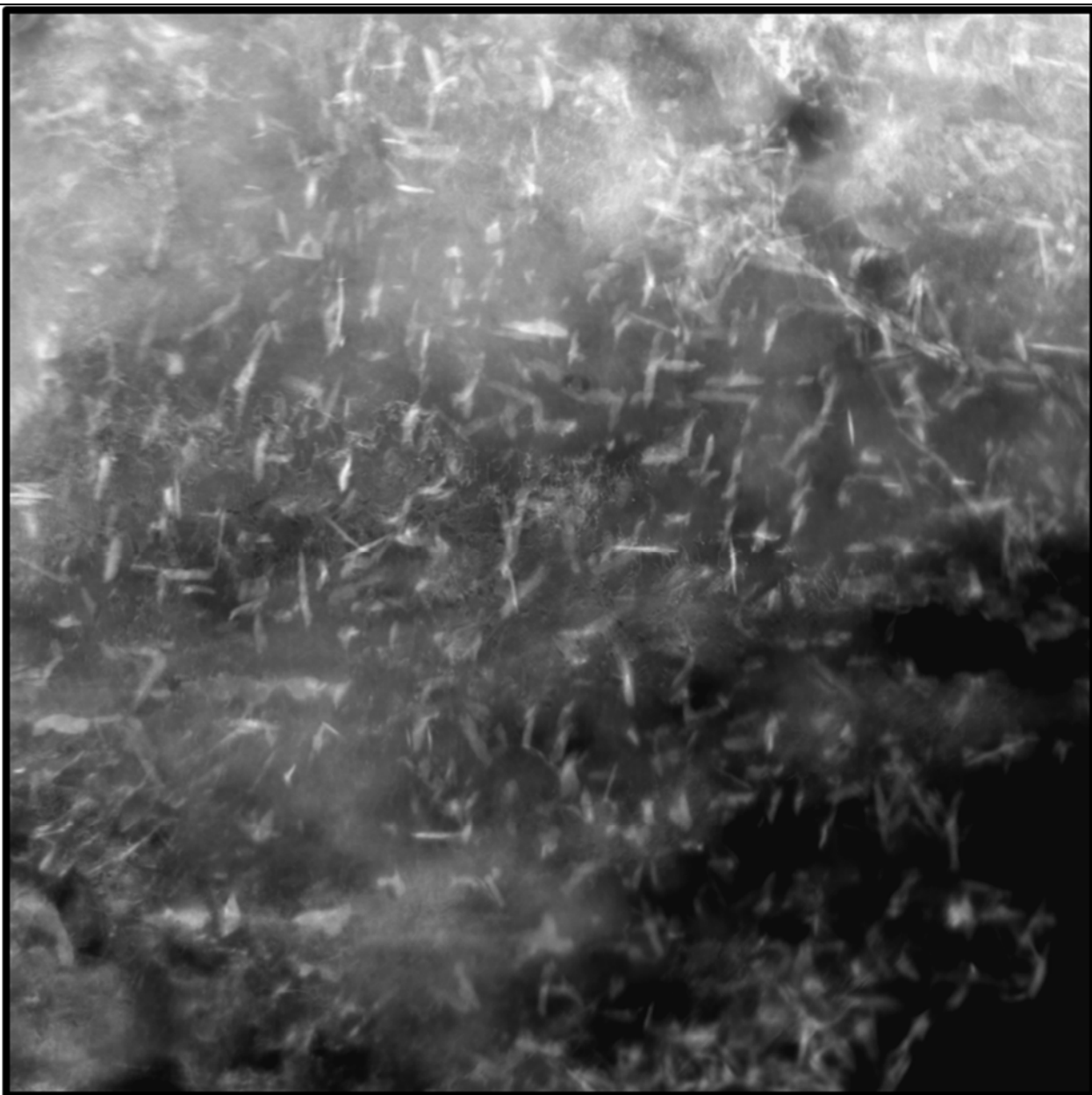
作品內容

將四元高熵合金均質化後作 70%冷加工並於 650°C 退火 1 小時所得之退火雙晶(白色)。

作者姓名: 林佑誼

學校單位: 國立台灣大學 材料所

E-Mail: r07527032@ntu.edu.tw



作品名稱 凍湖魚群

作品內容

自回火麻田散鐵之 STEM 影像，冰凍的湖面之下仍可見大量魚群暢遊。

作者姓名 曹梓敬

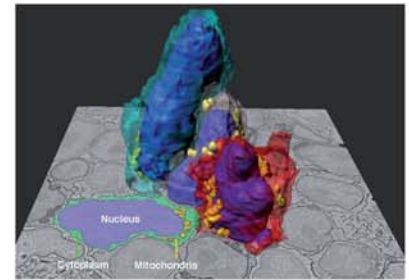
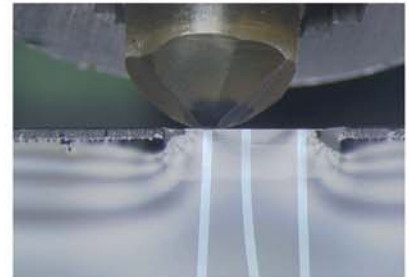
學校單位 臺灣大學材料所

E-Mail tctsao@ntu.edu.tw

3D影像重建 電顯超薄切片機

From Eye to Insight

Leica
MICROSYSTEMS



Get Quality Serial Sections for Array Tomography Fast

ARTOS 3D ULTRAMICROTOME

- > Ultramicrotome for automated serial sectioning used for subsequent 3D reconstruction
- > Automatically creates and collects hundreds of consistent, ultrathin serial-section ribbons
- > Sorts and positions a higher density of wrinkle-free ribbons, ready for optimized SEM analysis
Preserves section quality due to integrated direct sample transfer
- > The small size of a section carrier fits to every SEM chamber and is also an ideal solution for correlative light and electron microscopy (CLEM)

友聯光學有限公司 電話:(02)26980508
專線:0800-227123

Web: www.unionoptical.com.tw

www.leica-microsystems.com

BRUKER BRUKER獨特4合1電子顯微鏡分析組合



- **QUANTAX Micro-XRF:**
微量元素檢測(SEM用)
可以加裝在掃描電鏡上的Xtrace
微型X射線發射源。
使電子顯微鏡具備微區XRF分析能力。
- **QUANTAX EDS:** 最佳能量解析率
新一代的QUANTAX電致冷能譜儀
採用先進的 slim-line 技術。
可搭載不同有效面積的XFlash® 6探頭。
並具有超級數模雙通道脈衝處理器。

- **QUANTAX WDS:** 超高敏感度
具有精密結構的能譜儀設計。
完全馬達驅動的高級運動機構。
精密的自動光學中心定位系統。
與EDS無縫接軌的軟體系統。
- **QUANTAX EBSD:**
高速EBSD與EDS同步分析
可與 QUANTAX EDS 系統結合使用。
構成EBSD/EDS一體化同步分析系統。

ULVAC-PHI, INC. 世界領導品牌ULVAC-PHI

X光光電子能譜儀 XPS (X-ray Photoelectron Spectroscopy) 飛行時間二次離子質譜儀TOF-SIMS (Time of Flight Secondary Ion Mass Spectrometry) 歐傑電子能譜儀 AES (Auger Electron Spectroscopy)



VersaProbe III

- 專利設計之掃描式聚焦X光源，可產生類SEM影像
- 專利設計之雙射線束電性中和系統
- 最小X光射束可聚焦達10 μm以下
- 可擴充GCIB離子槍、C60離子槍、UPS 紫外光源配件、Auger 電子槍、Hot/Cold Stage 加熱/冷卻樣品平台、外加進樣系統等
- 五軸自動化控制之樣品平台



TRIFT V nano-TOF

- 專利設計之雙射線束電性中和系統
- 獨家三個半球型靜電分析器設計使離子飛行距離達兩公尺
- 表面粗糙樣品的容許度佳
- 五軸式電腦控制樣品平台
- 可同時加裝四個離子射源



PHI 710

- 專利的低電壓 Ar⁺ 濺鍍槍，對超薄層絕緣材料之縱深分析可有效中和表面電荷
- 獨家抗震及絕熱的設計，適合長時間的分析與提高影像的穩定性
- 提供無死角高解析度之二次電子影像及歐傑元素與化學態影像
- 專利設計之同軸式電子束與偵測器空間解析度佳，可得到精確的元素及化學態資訊



EDWARDS在真空系統領域為世界領導品牌，提供各種真空產品並遍及各個領域，以應對各種最新技術研發的挑戰。



- **nXDS Scroll Pumps**
具備優越的抽氣功能、擁有低極限壓力、低耗電量、低噪音、無油氣、低振動等特性。



- **nEXT 渦輪分子真空幫浦**
是多級軸流式渦輪機，高速旋轉葉片通過增加氣體在抽氣方向上移動的機率來提供高壓縮比。針對分子流動條件進行了優化，並且需要適當尺寸的前級幫浦將其排放到大氣中。



- **E2M 系列機械性油封幫浦**
具先進的潤滑迴路，高可靠性，以及各式配件符合特定應用需求。作為渦輪分子真空幫浦的前級，或提供一般實驗室之應用等皆可。



- **RV 系列小型油封迴轉葉片幫浦**
抽氣速率1.1 ~ 38.9 m³/h，終極壓力 2 × 10⁻³ mbar。抽吸速度良好，蒸氣處理能力優異，作業時順暢無聲。

thermo**scientific**

Scios 2 DualBeam System for Materials Science

Versatility and High-Performance

The Thermo Scientific™ Scios™ DualBeam™ System is an ultra-high resolution analytical system that provides outstanding sample preparation and 3D characterization performance for the widest range of samples, including magnetic and nonconductive materials. It is an ideal solution to meet the needs of scientists and engineers in advanced research and analysis in all environments.

Find out more at
[thermofisher.com/EM-materials-science](https://www.thermofisher.com/EM-materials-science)



ThermoFisher
SCIENTIFIC

© 2018 Thermo Fisher Scientific Inc. All rights reserved. All trademarks are the property of Thermo Fisher Scientific and its subsidiaries unless otherwise specified.